

Script - Lecture PHY 432

Physics with Muons: From Atomic Physics to Solid State Physics

Alex Amato

Contents

Literature	7
1. Introduction: the Muon	9
1.1. The muon: an elementary particle	9
1.2. Muon discovery	10
1.3. The pion: the parent particle	15
1.3.1. Pion properties	15
1.3.2. Pion production reactions	15
1.3.3. The pion decay	17
1.4. Muon properties	19
1.5. The muon decay	21
1.5.1. Generalities	21
1.5.2. Differential positron emission	21
1.5.3. Decay of a muon ensemble	24
1.6. Muon magnetic moment and spin precession	25
1.6.1. Muon magnetic moment	25
1.6.2. Muon spin precession	26
1.6.2.1. Classical view	26
1.6.2.2. Quantum mechanics view	27
1.7. Atmospheric muons	28
1.8. “Man-made” muons	34
1.8.1. Pion production: 3 different possible accelerators	34
1.8.2. Pion production: for example at the Paul Scherrer Institute	36
1.8.3. Muon beams for condensed matter	40
1.8.3.1. “High-energy” muons	40
1.8.3.2. “Surface” muons	44
1.8.3.3. Few words about a typical beamline and beam optics	46
1.8.3.3.1. Dipole magnets	47
1.8.3.3.2. Quadrupole magnets	48
1.8.3.3.3. Separator (Wien filter) and spin rotator	53
2. Implanting Muons in Matter	57
2.1. Energy loss of particles in matter	57
2.1.1. Energy loss by ionization: classical approach	59
2.1.2. Energy loss: Bethe formula	62
2.2. Range and thermalization time	68
2.2.1. Range of muons	68
2.2.2. Thermalization time	71
2.3. “Free” muon vs muonium	72

3. μSR Technique	75
3.1. The μ SR signal	76
3.2. Key features of the μ SR technique	81
3.2.1. Local probe - volume sensitivity	81
3.2.2. Larmor frequency - magnetic field sensitivity	84
3.2.3. Typical time window	85
3.2.4. Other important features	85
3.3. Experimental setup	87
3.3.1. At a “continuous-wave” (cw) beam	87
3.3.2. At a pulsed beam	92
3.3.3. Muon-on-request setup	93
3.4. The different measurement geometries	94
3.4.1. ZF & LF geometry	94
3.4.2. TF geometry	97
4. Depolarization Functions	99
4.1. Depolarization function for static internal fields (ZF geometry)	99
4.1.1. The simple case: single value of field	101
4.1.1.1. Single-crystal case	101
4.1.1.1.1. Some examples	103
4.1.1.2. Polycrystal case	105
4.1.1.2.1. Some examples	107
4.1.2. Randomly oriented fields	110
4.1.2.1. Gaussian distribution	110
4.1.2.1.1. Some examples	113
4.1.2.2. Lorentzian distribution	115
4.1.2.2.1. Some examples	117
4.1.2.3. “In between”	117
4.1.3. Generalization	118
4.2. Depolarization function for applied external fields (TF geometry)	119
4.3. Dynamical effects	121
4.3.1. The strong collision approximation	121
4.3.2. The muon depolarization	123
4.3.2.1. Approximations for some limiting cases	125
4.3.3. Examples	126
4.3.4. Testing for the dynamical character LF external field	129
5. Studying magnetism with the μSR technique	137
5.1. Local magnetic fields in magnetic materials	137
5.1.1. The interaction muon - electron	137
5.1.2. Dipolar and contact contributions	138
5.1.2.1. Orbital field	138
5.1.2.2. Dipolar field	138
5.1.2.3. Contact field	141
5.1.3. Demagnetizing field and Lorentz sphere	142
5.2. Examples of magnetic states studied by μ SR	145

5.3.	Special cases magnetic states	157
5.3.1.	Incommensurate vs commensurate magnetic structure	157
5.3.1.1.	The simple case	157
5.3.1.2.	The slightly more difficult case	161
5.3.2.	Study of spin glasses	164
5.4.	Determining magnetic volume fractions	165
5.5.	Studying the magnetic response in the paramagnetic or diamagnetic states: the Knight shift	168
5.5.1.	Knight shift (contact term): Studying the paramagnetism of the con- duction electrons	169
5.5.1.1.	Pauli susceptibility	170
5.5.2.	Knight shift in materials with local moments	174
5.5.2.1.	The dipole field contribution	174
5.5.2.2.	The enhanced contact field contribution	175
5.5.2.3.	The total Knight shift	176
5.5.3.	Determining the muon-stopping site	177
5.6.	Depolarization created by nuclear moments	182
5.6.1.	Classical calculation	182
5.6.1.1.	The TF case	182
5.6.1.2.	The ZF case	185
5.6.1.3.	Comment	187
6.	μSR in the Superconducting State	189
6.1.	Introduction	189
6.2.	Two characteristic lengths in superconductors	191
6.2.1.	The magnetic penetration depth	192
6.2.1.1.	The London equations	192
6.2.1.2.	Field and current decay in the Meissner state	193
6.2.2.	The coherence length	195
6.2.2.1.	The Ginzburg Landau theory	195
6.3.	Two types of superconductor	198
6.3.1.	Condensation energy and energy balance	198
6.3.2.	Type I and type II superconductors	199
6.4.	Abrikosov state of a type II superconductor	202
6.4.1.	Field in the Abrikosov state	203
6.4.1.1.	Field due to one vortex	205
6.4.1.2.	Field distribution of an extreme type II superconductor	206
6.4.1.3.	Corrections due to the coherence length and the magnetic field	209
6.5.	Obtaining the characteristic lengths from μ SR	214
6.5.1.	Obtaining the penetration depth	214
6.5.1.1.	Multi-Gaussian approach	218
6.5.2.	Obtaining the coherence length	220
6.6.	Testing the superconducting gap symmetry	221
6.7.	Determining the anisotropy of the magnetic penetration depth	225
6.8.	Multiple superconducting gaps	226
6.9.	Uemura relation, Uemura plot: Correlation between T_c and σ	227

6.10. Dynamics of the FLL	230
6.10.1. Melting through temperature	230
6.10.1.1. Stabilization with defects	230
6.10.2. Moving the FLL with an applied current	230
7. Low energy muons: a tool to study thin films and heterostructures	231
7.1. Introduction	231
7.2. Generation of low energy muons	232
7.2.1. Moderation in thin layers of cryosolids	232
7.2.2. Laser resonant ionization of muonium	235
7.3. The Low-Energy Muon (LEM) instrument at PSI	235
7.4. Stopping profiles of Low-Energy Muons in thin films	237
7.5. Examples of LEM studies	237
7.5.1. Magnetic field penetration at the surface of superconductors	237
7.5.2. In-plane anisotropy of the magnetic penetration depth in ultra clean $\text{YBa}_2\text{Cu}_3\text{O}_{6.92}$	237
7.5.3. Giant proximity effect in cuprate heterostructures	237
7.5.4. Probing the spin injection in an organic spin valve	237
8. Muonium	239
8.1. Introduction	239
8.2. Properties	239
A. Annex	241
A.1. Magnetic Moment	241
A.1.1. Introduction	241
A.1.2. Relation to the angular momentum	242
A.1.2.1. Orbital angular momentum	242
A.1.2.2. Spin angular momentum	243
A.2. Spin Angular Momentum	243
A.2.1. Spin Operators	243
A.2.2. Spin Space	244
A.2.3. Eigenstates of S_z and S^2	246
A.2.4. Pauli Representation	247
A.2.5. Relating Spinor to Spin Direction	250
A.3. The canonical momentum (or generalized momentum)	251
A.3.1. Legendre transformation	252
A.3.2. Rewriting the Hamiltonian	253
A.4. The demagnetizing field	254
Bibliography	257

Forwords

The first version of this lecture notes was composed in December 2017 and Januar 2018. Though I have presented the topics my way, the script is in a large part based on the excellent previous notes composed by Elvezio Morenzoni (see <https://www.psi.ch/lmu/lectures>). Also, I took profit of many valuable inputs and available documents authored by my colleagues at the Laboratory for Muon Spin Spectroscopy of the Paul Scherrer Institute. Among them, I would like to specially thank Hubertus Luetkens, Thomas Prokscha, Andreas Suter and Rustem Khasanov. I would like to thank also Daniel Andreica (Cluj-Napoca University) for discussions about the concept and finally Karla Mihov (Humboldt-Universität zu Berlin) for useful inputs about, and a critical reading of, the first version of the script.

Alex Amato

Literature

Books

- A. Yaouanc, P. Dalmás de Réotier
Muon Spin Rotation, Relaxation and Resonance
Oxford University Press, 2011
- E. Karlsson
Solid State Phenomena, As Seen by Muons, Protons, and Excited Nuclei
Clarendon, Oxford, 1995
- S.L. Lee, S.H. Kilcoyne, R. Cywinski (eds.)
Muon Science: Muons in Physics; Chemistry and Materials
IOP Publishing, Bristol and Philadelphia, 1999
- A. Schenck
Muon Spin Rotation Spectroscopy
Adam Hilger, Bristol, 1985

Introductory articles

- S.J. Blundell
Spin-Polarized Muons in Condensed Matter Physics
Contemporary Physics 40, 175-192 (1999)
- P. Bakule, E. Morenzoni
Generation and Application of Slow Polarized Muons
Contemporary Physics 45, 203-225 (2004)
- A. Amato and D. Andreica
Muon Spin Rotation
in: Encyclopedia of Condensed Matter Physics, ed. by F. Bassani *et al.*, Elsevier, Oxford (2005) Pages 41-49
- A. Amato
Muon Spin Rotation (μ SR): Applications in Magnetism

in: Encyclopedia of Materials: Science and Technology (Second Edition) 2001, Pages 5888-5892

Reviews articles: applications

- P. Dalmas de Réotier and A. Yaouanc
Muon Spin Rotation and relaxation in Magnetic Materials
J. Phys. Condens. Matter 9, 9113-9166 (1997)
- A. Schenck and F.N. Gygax
Magnetic Materials Studied by Muon Spin Rotation Spectroscopy
in: *Handbook of Magnetic Materials*, edited by K.H.J. Buschow, Vol. 9, Pages 57-302
Elsevier, Amsterdam, 1995
- B.D. Patterson
Muonium States in Semiconductors
Rev. Mod. Phys. 60, 69-159 (1988)
- A. Amato
Heavy-Fermion Systems Studied by μ SR Techniques
Rev. Mod. Phys., 69, 1119-1179 (1997)
- V. Storchak, N. Prokovev
Quantum Diffusion of Muons and Muonium Atoms in Solids
Rev. Mod. Physics, 70, 929 (1998)
- J. Sonier, J. Brewer, R. Kiefl
 μ SR Studies of Vortex State in Type-II Superconductors
Rev. Mod. Physics, 72, 769 (2000)
- E. Roduner
The Positive Muon as a Probe in Free Radical Chemistry
Lecture Notes in Chemistry No. 49
Springer Verlag, Berlin, 1988

1. Introduction: the Muon

1.1. The muon: an elementary particle

The muon (μ) is one of the few elementary particles, possessing a unit electric charge and a spin $1/2$. It is a *charged lepton*, that is an elementary particle which does not participate in the strong interaction. Note that the muon particle has a negative charge, whereas the antimuon (μ^+) has a positive charge. In the following we will simply speak about negative and positive muons.

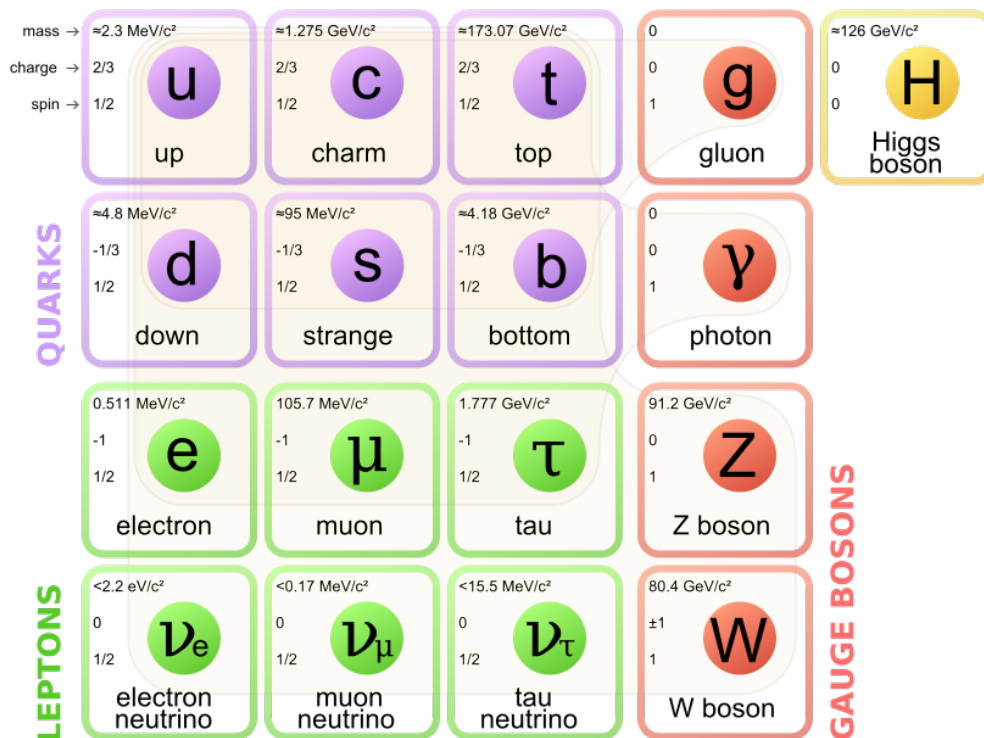


Figure 1.1.: Standard model of elementary particles: the 12 fundamental fermions (half-integer spin $1/2$) and 4 fundamental bosons (integer spin). Brown loops indicate which bosons (red) couple to which fermions (purple and green). Note that the gauge boson Graviton is still a hypothetical elementary particle (i.e. not shown) that mediates the force of gravitation in the framework of quantum field theory. Note also that the term elementary particle just indicate that the substructure of this particle is unknown, thus it is unknown whether it is composed of other particles. (Taken from https://en.wikipedia.org/wiki/Elementary_particle.)

1.2. Muon discovery

- 1785 Charles Augustin de Coulomb found that electroscopes can spontaneously discharge by the action of the air and not by defective insulation.
- 1850 In 1850, Italian physicist Canò Matteucci and later British physicist William Crookes in 1879 showed that the rate of spontaneous discharge decreased at lower atmospheric pressures.
- 1896 Becquerel discovered natural radioactivity. The discovery of radioactivity triggered interest about the origin of the spontaneous electrical discharge observed earlier in the air. The obvious hypothesis was that the discharge was caused by the radioactive materials on Earth, though this was difficult to prove.
- 1899 Elster and Geitel found that surrounding a gold leaf electroscope with a thick metal box would decrease its spontaneous discharge. From this observation, they concluded that the discharge was due to highly penetrating ionizing agents outside of the container.
- 1909-1910 Theodor Wulf performed experiments with precise electrometers, which detected natural radiation sources on the ground. Wulf took his electroscope to the top of the Eiffel tower. Actually he wanted to test whether the radiation was coming from the Earth. He found that the intensity of radiation *decreases at nearly 300 m [altitude to] not even to half of its ground value*, but the results were not really conclusive.
- 1910 Albert Gockel (Uni. Fribourg) arranged the first balloon flights with the purpose of studying the properties of penetrating radiation.¹ Albert Gockel, measured the levels of ionizing radiation up to a height of 3000 meters. He concluded that the ionization did not decrease with height and consequently could not have a purely terrestrial origin. He also introduced the term “kosmische Strahlung” (cosmic radiation).
- 1907-1911 Domenico Pacini observed that ionization underwater was significantly lower than on the sea surface. For these measurements he immersed an electroscope 3 m deep in the sea at Livorno. This demonstrates that part of the ionization itself must be due to sources other than the radioactivity of the Earth. Pacini concluded that “...*sizable cause of ionization exists in the atmosphere, originating from penetrating radiation, independent of the direct action of radioactive substances in the ground*” [1].

¹See for example

<http://www.sps.ch/artikel/geschichte-der-physik/albert-gockel-from-atmospheric-electricity-to-cosmic-radiation-5/>



Figure 1.2.: *Domenico Pacini.*

Taken from https://commons.wikimedia.org/wiki/File%3APacini_measurement.jpg

1911-1912 Victor Hess makes measurements from balloons up to an altitude of 5.2 km. He measures an increasing charge with increasing altitude.



Figure 1.3.: *Victor F. Hess, center, departing from Vienna about 1911.*

1913 The results by Hess were confirmed by the young Werner Kolhörster during different flights up to 9.2 km.

1924-1926 Millikan first questioned the existence of cosmic rays after flight above Texas up to 15 km (the results were blurred by the latitude geomagnetic effect, see below). “*We conclude, therefore, that there exists no such penetrating radiation as we have assumed*” [2].

By using unmanned balloons to perform experiments at even higher altitude, Millikan

completely changed his mind and coins the expression ‘cosmic rays’. “... *all this constitutes pretty unambiguous evidence that the high altitude rays do not originate in our atmosphere, very certainly not in the lower nine-tenths of it, and justify the designation ‘cosmic rays’*” [3].

Backed by US media, Millikan moved to take the glory of the discovery, which triggered an angry answer by Hess [4]: “...*The recent determination by Millikan and his colleagues of the high penetrating power of high-altitude radiation has been an occasion for American scientific journals such as ‘Science’ and ‘Scientific Monthly’ to propose to name the name ‘Millikan Rays’.* As his work is merely a confirmation and extension of the results obtained by Gockel, myself and Kolhörster from 1910 to 1913 using balloon borne measurements of the rays, this appellation should be rejected as it is misleading and unjustified....

1927 The geomagnetic effect on the cosmic rays was discovered by J. Clay [5]. As the interstellar charged particles that approach at the level of the equator have to travel in a direction perpendicular to the earth magnetic field, they are deflected away through the Lorentz force and only very energetic particles reach the earth. Near the poles, incoming particles have a higher probability that their trajectory is along the magnetic lines and therefore will not sense the Lorentz force.

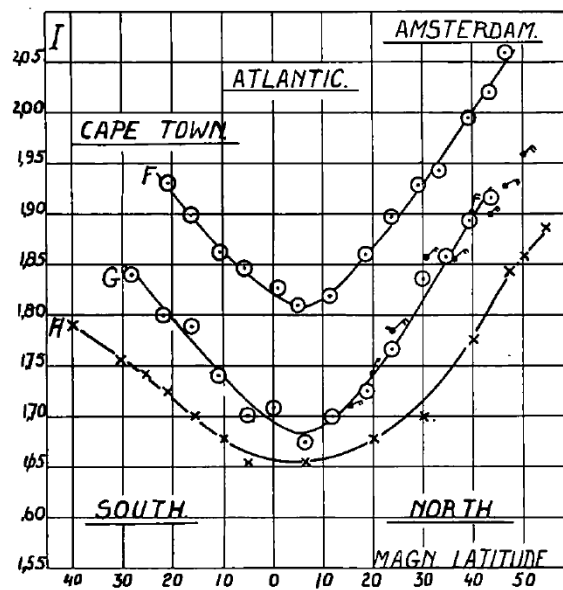


Figure 1.4.: Change of cosmic radiation as a function of the latitude [5].

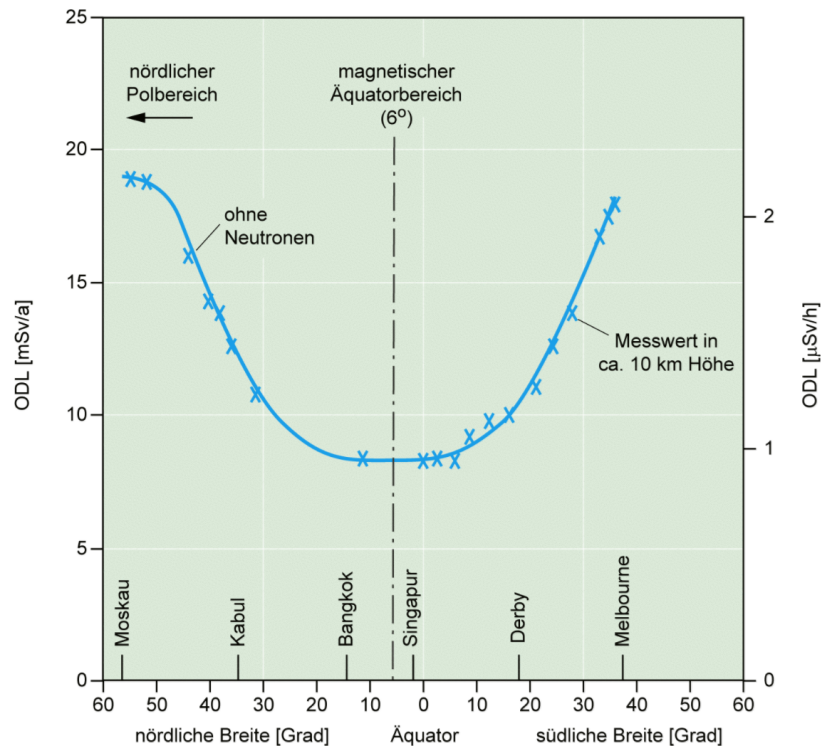


Figure 1.5.: Same experiment performed during an aircraft flight in 1988 from Melbourne to Frankfurt [6]. Note that the radiation does not disappear near the magnetic equator, as the geomagnetic effect has a larger impact on the part of the cosmic ray with relatively low energy, i.e. the plasma coming from the sun.

1933 First muon picture (but not correctly identified) in a Wilson cloud chamber by Kunze [7].

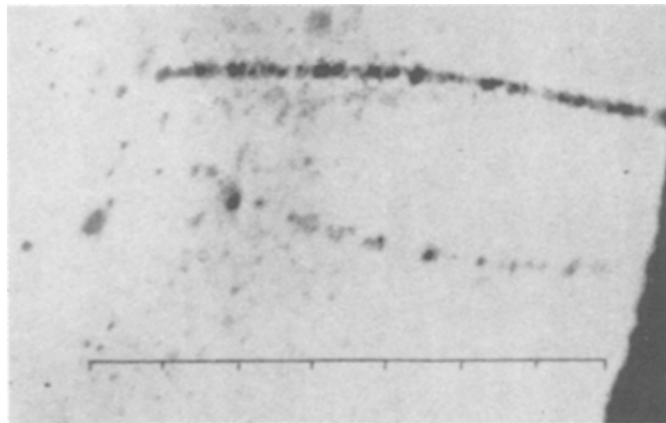


Fig. 5.

Doppelspur als Resultat einer vermutlichen Kernexplosion.
7-fache Vergrößerung. Untere Spur = Elektron von 37 000 000 V.
Natur der oberen positiven Korpuskel nicht sicher bekannt.

Figure 1.6.: First observation of a muon (not identified) [7]. The original figure caption is also reported.

- 1936 V. Hess receives the Nobel Prize for the discovery of cosmic radiation.
- 1936-1937 Discovery of the muon by C. Anderson and S. Neddermeyer using a cloud chamber to an altitude of 4300 m on Pike's Peak [8]. They gave it the name 'mesotron'. The muon however was first misinterpreted as the so-called H. Yukawa's particle [9] mediating the nuclear force (residual strong interaction between hadrons).
- 1941 B. Rossi and D.B. Hall [10] determine the muon life time to be $\tau_\mu = (2.4 \pm 0.3) \times 10^{-6}$ s.
- 1945-1947 Conversi *et al.* [11] measure the lifetime of positive and negative muons. The lifetime is too long for strongly interacting particles. It turns out that the Yukawa's particle is actually the pion.
- 1946 Discovery of the pion by C.F. Powell *et al.* [12] studying the cosmic rays using specialized photographic emulsions at high-altitude. **The pion**, which proved to be the Yukawa's particle, **primary decays into a muon and a muon neutrino** (see Section 1.3.1).
- 1946 T.D. Lee and C.N. Yang [13] predicted that any process governed by the weak interaction should lead to a violation of parity. The Nobel Prize in Physics 1957 was awarded jointly to them.
Between Christmas of 1946 and New Year's, National Bureau of Standards (NBS) scientists led by Columbia Prof. C.S. Wu. [14] confirmed that the emission of beta particles is asymmetric for cobalt-60 nuclei oriented with a strong magnetic field.
- 1957 R. Garwin *et al.* [15] measure **the parity violation in weak decay of the muon** [16]. This work was followed by the one of Friedman *et al.* few months later [15].
Garwin *et al.* made the following remark: *It seems possible that polarized positive and negative muons will become a powerful tool for exploring magnetic fields in nuclei [...], atoms, and interatomic regions*, hence predicting the later use of muons by solid state physicists.

1.3. The pion: the parent particle

1.3.1. Pion properties

The generic name pion is for any of the particles π^- , π^+ and π^0 . The pion is classified as a meson as it consists of a quark and an antiquark (u and d quark). As proposed by Hideki Yukawa [9], the exchange of virtual pions provides an explanation for the residual strong force between nucleons. Pions are produced in high energy accelerators in collisions between hadrons (see Section 1.3.2). Pions are also produced in nature when high energy cosmic rays enter in the Earth's atmosphere.

Table 1.1.: *Main properties of the pion.*

	π^+	π^-	π^0
Lifetime (s)	$26.033 \pm 0.005 \times 10^{-9}$	$26.033 \pm 0.005 \times 10^{-9}$	$8.4 \pm 0.6 \times 10^{-17}$
Spin	0	0	0
Mass (MeV/ c^2)	139.57018 ± 0.00035	139.57018 ± 0.00035	134.9766 ± 0.0006
Decay	$\rightarrow \mu^+ + \nu_\mu$	$\rightarrow \mu^- + \bar{\nu}_\mu$	$\rightarrow \gamma + \gamma$

1.3.2. Pion production reactions

Pions are not produced in radioactive decay, but are produced through high energy collisions between hadrons. These collisions happen either in natural processes, for example when high energy cosmic ray protons interact with matter in the Earth's atmosphere, or in high energy accelerators.

The production of pions occurs through the collision of nucleons with sufficient energy involved, *i.e.* with an available energy in the center of mass exceeding the rest pion mass (see Table 1.1). Typical reactions to produce a single positive pion are for example:

$$p + p \rightarrow p + n + \pi^+ \quad (1.1)$$

$$p + n \rightarrow n + n + \pi^+ \quad (1.2)$$

Even though the neutral pion mass is 135 MeV/ c^2 (see Table 1.1) an incoming proton with 135 MeV of kinetic energy will not be able to create a neutral pion in a collision with a proton of the target. This is due to the conservation of momentum.

The simplest way to figure the necessary energy the incoming proton needs to create a neutral pion is to calculate in the **center of mass frame** (see exercise). In this frame the least possible kinetic energy must be just enough to create the neutral pion with the final state particles at rest. One finds that the necessary velocity of the proton (in the center mass frame) must be

0.36c. We need to know the energy necessary in the “lab” frame, *i.e.* that in which one of the protons is initially at rest. Using the relativistic addition of velocities formula, we obtain 0.64c. This implies the incoming proton has a kinetic energy around 280 MeV.

Thus to create a pion of rest energy 135 MeV, it is necessary to give the incoming proton at least 280 MeV of kinetic energy. This is called the “threshold energy” for pion production. The “inefficiency” arises because momentum is also conserved, so there is still considerable kinetic energy in the final particles. As shown on Fig. 1.7 the optimum energy for pion production is above 500 MeV (corresponding to the maximum of the cross section). This defines the energy of an accelerator needed to produced pion (and muon) beams.

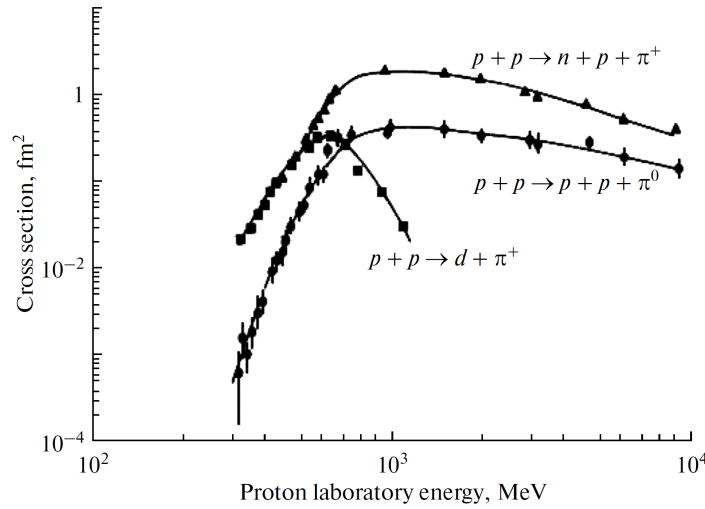


Figure 1.7.: Energy dependence of the cross section² for pion production in some nucleon-proton reactions.

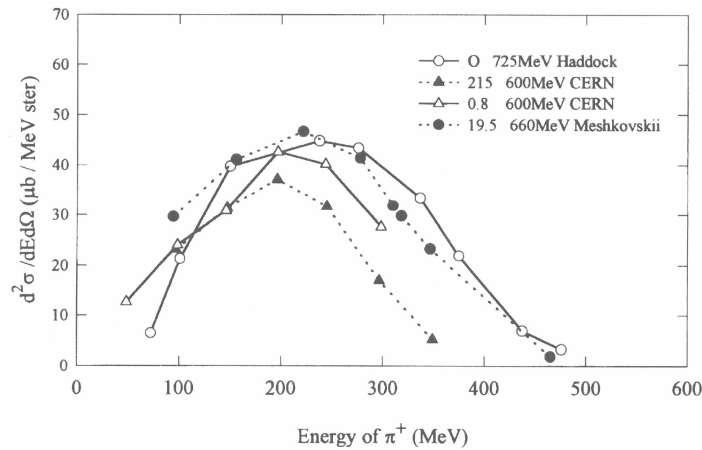


Figure 1.8.: Double differential production cross section as a function of the positive pion energy.

²The cross section can be considered as the effective area for the collision, *i.e.* it is often used to mean the probability that two particles will collide and react. The natural unit of the cross section is of course m², but the cross section is often given in barn, with 1 b = 10⁻²⁸ m² = 100 fm².

For a maximum number of single pions the incident proton beams should have energies in the range 500 MeV to 1000 MeV. At higher energies, it is possible to have reactions producing a pair of pions. However, the “threshold energy” is here of the order of 600 MeV with the cross section reaching a saturation above 1.5 GeV.

1.3.3. The pion decay

In this Section we will concentrate on the decay of the positive pion.

As seen in Table 1.1, the pion life-time is about 26 ns and the primary decay mode, with a branching fraction of 0.999877, is a leptonic decay into a muon and a muon neutrino:

$$\pi^+ \rightarrow \mu^+ + \nu_\mu \quad (1.3)$$

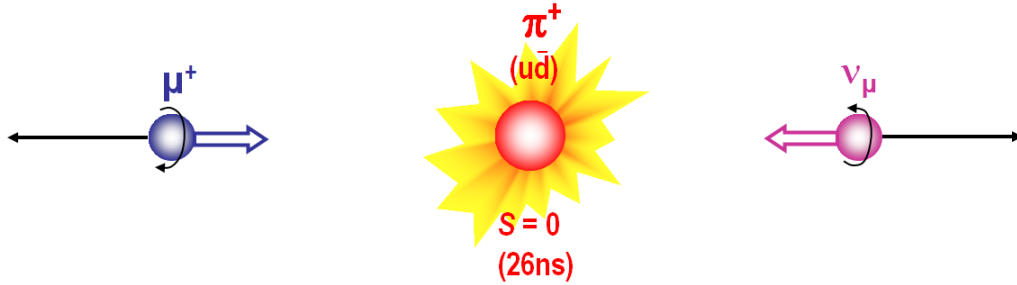


Figure 1.9.: Schematic of a pion decay. The black arrows represent the flying paths and the colored arrows represents the particle spins.

Two points are important in this decay process.

1. It is a two-body decay, then the conservation of momentum and energy leads to important features. Hence, the muon and neutrino fly in opposite directions in the reference frame of the pion. Also the decay products have definite energies. The muon has always the energy 4.1 MeV (\rightarrow Exercises) in the reference frame of the pion (assuming that the neutrino has a mass $m_\nu = 0$).
2. The pion has a spin $S = 0$. The total spin is conserved during the decay. As only left-handed neutrinos are produced in nature, this has as consequence that the muon has a spin $S = 1/2$ and is 100% polarized.

The decay proceeds by the weak interaction³. During the decay a parity violation occurs: this is evidenced by the fact that no neutrino with helicity -1 exist and therefore the parity operation of the pion decay (see Fig. 1.9) does not exist.

³The weak interaction involves the exchange of the intermediate vector bosons, the W and the Z (in this case a boson W^+). It has a range of about 10^{-18} meter which is about 0.1% of the diameter of a proton. We will not treat the weak interaction, which goes beyond the scope of the lecture. A discussion of the weak interaction can be found in Ref. [17] and on Ref. [18] for the muon decay (pages 29 to 36).

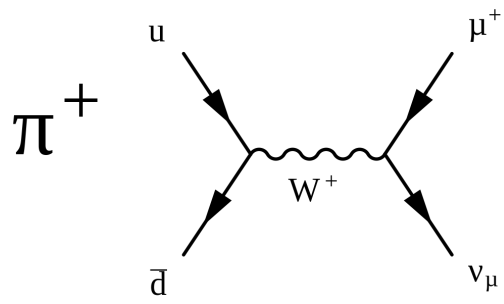


Figure 1.10.: *Feynman diagram of the pion decay. The pion is composed by the u and \bar{d} quarks.*

1.4. Muon properties

Table 1.2 provides the main muon properties which will be important to perform muon-spin spectroscopy experiments. We can identify several crucial points:

Table 1.2.: *Main properties of the muon.*

Lifetime (s)	$2.1969811(22) \times 10^{-6}$
Charge	$+e$ (or $-e$ for the μ^-)
Spin I_μ	$1/2$
Magnetic Moment	$\mu_\mu = 4.836 \times 10^{-3} \mu_B$ ($1 \mu_B = 9.274009994(57) \times 10^{-24}$ J/T) $3.18 \times \mu_p$ $8.9 \times \mu_N$
Gyromagnetic ratio γ_μ	$2\pi \times 135.538817$ MHz/T
Mass	$105.6583745(24)$ MeV/ c^2 $206.768 \times m_e$ $0.1124 \times m_p$
Principal decay	$\rightarrow e^+ + \nu_e + \bar{\nu}_\mu$

- The muon is a *purely magnetic* probe.
Classically the electric quadrupole moment of an entity of charge e and charge density ρ is given by

$$Q = \int (3z^2 - r^2) \rho(r) d^3r . \quad (1.4)$$

For a spherical distribution of charge, $\langle x^2 \rangle = \langle y^2 \rangle = \langle z^2 \rangle = 1/3 \times \langle r^2 \rangle$, and the quadrupole moment vanishes.⁴

⁴ In the quantum mechanics, the approach can be made by noting that

$$Q = Q_{20} = \int (3z^2 - r^2) \rho(r) d^3r = \sqrt{\frac{16\pi}{5}} \int r^2 Y_2^0 \rho(r) d^3r , \quad (1.5)$$

where Y_2^0 is the spherical function with $\ell = 2$ and $m = 0$.

In the quantum mechanics the quadrupole moment is defined as the expectation value of the quadrupolar tensor $e(16\pi/5)^{1/2} r^2 Y_2^0$ in the substate $|I, M = I\rangle$.

At this point it is useful to use the Wigner-Eckhart Theorem, where:

$$\langle J M | T_{(k)}^q | J' M' \rangle = \langle J' M' k q | J M \rangle \langle J || T_{(k)} || J' \rangle , \quad (1.6)$$

where $T_{(k)}^q$ is the q -th component of the spherical tensor operator $T_{(k)}$ of rank k (in our case $k = 2$), $\langle J' M' k q | J M \rangle$ is the ‘‘Clebsch-Gordan’’ coefficient for coupling J' with k to get J , and $K = \langle J || T_{(k)} || J' \rangle$ is a value that is called the ‘‘reduced matrix element’’. This means that the matrix element of a tensor operator can be factored into a part which is independent of the tensor itself, but involves the projection quantum numbers (‘‘Clebsch-Gordan’’ coefficient), and a part not involving the projection quantum numbers (‘‘reduced matrix element’’). Since the reduced matrix element is common to all the states differing only by

- The muon magnetic moment (or in other words the gyromagnetic ratio) is large making the muon a very sensitive magnetic probe.
- The muon life time is short but still easily accessible with modern detector and timing techniques.
- The decay into a positron and neutrinos represents a branching fraction of basically 100%. Other possible decays involve either a positron and a gamma ($\rightarrow e^+ + \nu_e + \bar{\nu}_\mu + \gamma$) or 2 positrons and an electron ($\rightarrow e^+ + \nu_e + \bar{\nu}_\mu + e^+ + e^-$).

their M and q -values, there is only one single independent quantity characterizing multipole coefficients of order k for all $2J + 1$ magnetic substates. It is therefore convenient to define the multipole moment as the expectation value in the state of maximum M (*i.e.* $M = I$).

We have therefore:

$$Q = e \sqrt{\frac{16\pi}{5}} \langle I, M = I | r^2 Y_2^0 | I, M = I \rangle \propto \langle I, M = I | 20 | I, M = I \rangle \times K \propto \sqrt{I(2I-1)} \quad , \quad (1.7)$$

where $\langle I, M = I | 20 | I, M = I \rangle$ is the appropriate Clebsch-Gordan coefficient and K the reduced matrix coefficient independent of M . Therefore, for either $I = 0$ and $I = 1/2$ (for example the muon) the quadrupolar interaction vanishes.

1.5. The muon decay

1.5.1. Generalities

As said, muons is an unstable particle and decays with a mean lifetime of $\tau_\mu \simeq 2.197 \mu\text{s}$ as follows

$$\begin{aligned}\mu^+ &\rightarrow e^+ + \nu_e + \bar{\nu}_\mu \\ \mu^- &\rightarrow e^- + \bar{\nu}_e + \nu_\mu .\end{aligned}\quad (1.8)$$

As this is a three-body decay, the kinetic energy of the emerging positron⁵ may take values varying continuously from zero up to a maximum value $E_{e^+, \text{max}}$.

The case of zero kinetic energy represents the situation where the neutrino and antineutrino emerge antiparallel and carry away all the available kinetic energy. On the other hand side, the kinetic energy of the positron is maximum when the neutrino and antineutrino travel together in the direction opposed to the one of the positron.

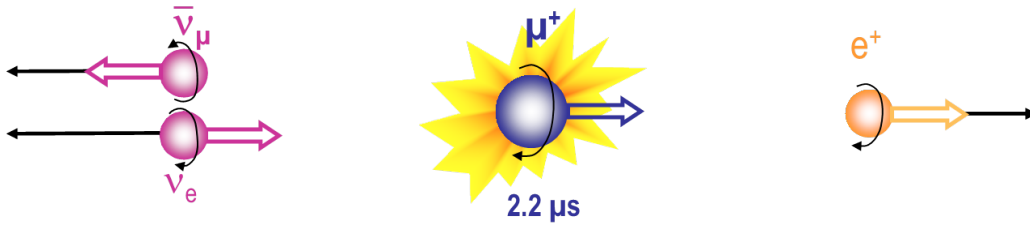


Figure 1.11.: Schematic of a positive muon decay. The black arrows represent the flying paths and the colored arrows represents the particle spins. the situation represents a decay producing a positron of maximum energy.

The maximum and mean positron energies resulting from the three body decay are given by (see Exercices):

$$E_{e^+, \text{max}} = \frac{m_\mu^2 + m_e^2}{2m_\mu} c^2 = 52.82 \text{ MeV} \quad \text{and} \quad (1.9)$$

$$\bar{E}_{e^+} = 36.9 \text{ MeV} . \quad (1.10)$$

1.5.2. Differential positron emission

The quantitative treatment of the muon decay is based on the weak interaction and we are interested by the differential positron emission probability per unit of time as function of the

⁵We concentrate the discussion on the positive muons, but the considerations are analog for the negative ones.

energy and solid angle, which is given by [19]

$$d\Gamma = W(\varepsilon, \theta) d\varepsilon d\Omega = \frac{1}{4\pi\tau_\mu} 2\varepsilon^2(3-2\varepsilon) \left[1 + \frac{2\varepsilon-1}{3-2\varepsilon} \cos\theta \right] d\varepsilon d\Omega , \quad (1.11)$$

where we have $\varepsilon = E_{e^+}/E_{e^+, \max}$, and $d\Omega = \sin\theta d\theta d\phi$ is the solid angle (with here θ is the polar angle and ϕ is the azimuthal one). We see that $d\Gamma$ is independent of ϕ .

The important point in Eq. 1.11 is the energy dependent asymmetry term

$$a(\varepsilon) = \frac{2\varepsilon-1}{3-2\varepsilon} , \quad (1.12)$$

which is a direct consequence that the muon decay is governed by the weak interaction. Therefore the positrons are emitted asymmetrically around the muons. As we will see in Section 3 this asymmetric positron emission is the key feature at the base of the μ SR technique.

With this definition, we can rewrite the Eq. 1.11

$$\begin{aligned} d\Gamma &= W(\varepsilon, \theta) d\varepsilon d\Omega = \frac{1}{4\pi\tau_\mu} 2\varepsilon^2(3-2\varepsilon) [1 + a(\varepsilon) \cos\theta] d\varepsilon d\Omega \\ &= \frac{1}{4\pi\tau_\mu} E(\varepsilon) [1 + a(\varepsilon) \cos\theta] d\varepsilon d\Omega . \end{aligned} \quad (1.13)$$

We can understand this asymmetry term, by considering the situation for positrons emitted with kinetic energies of the order of $E_{e^+, \max}$. Those positrons can be considered as ultra-relativistic antiparticles (recall that the mass of the positron is $0.511 \text{ MeV}/c^2$) for which the Dirac theory tells us that these antiparticles behave as antineutrinos with helicity $h = 1$, *i.e.* with a spin pointing in the propagation direction (see Fig. 1.11). Therefore, we see that for high energy positron, in order to conserve the spin during the muon decay process, the positron emission direction will be preferentially along the muon spin direction (*i.e.* asymmetric). We see that for $\varepsilon \rightarrow 1$ then $a(\varepsilon) \rightarrow 1$, *i.e.* we have a maximum asymmetry. On the other hand side, the asymmetry disappears for $\varepsilon = 1/2$ and becomes even negative for lower positron energies.

We can see first that if we integrate Eq. 1.11 over the energy and the solid angle (*i.e.* the angles θ and ϕ) we get the total decay rate

$$\Gamma = \int_0^{2\pi} \int_0^\pi \int_0^1 W(\varepsilon, \theta) d\varepsilon \sin(\theta) d\theta d\phi = \frac{1}{\tau_\mu} , \quad (1.14)$$

as we should.

We can now look at the rate as a function of the energy, *i.e.* the energy spectrum of the positrons independent of the emission angle. This is of course obtained from Eq. 1.11 by integrating over the angles θ and ϕ (see Fig. 1.12)

$$d\Gamma = W(\varepsilon) d\varepsilon = \frac{1}{\tau_\mu} 2\varepsilon^2(3-2\varepsilon)d\varepsilon = \frac{1}{\tau_\mu} E(\varepsilon)d\varepsilon . \quad (1.15)$$

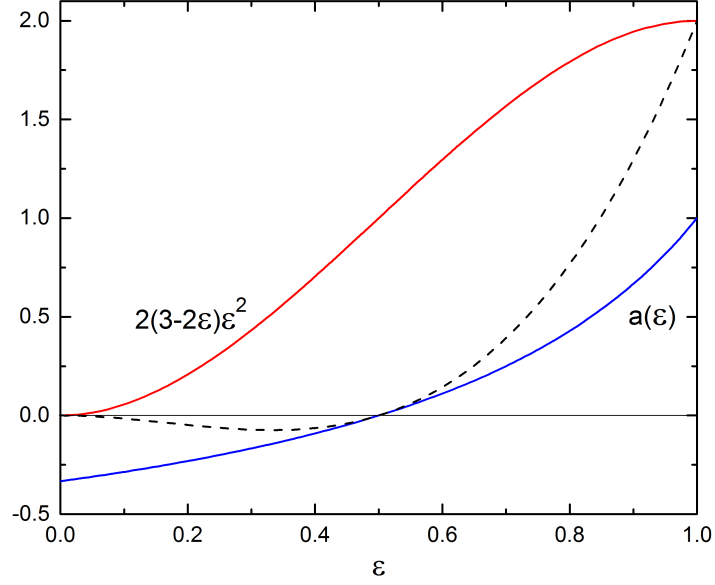


Figure 1.12.: *Normalized energy spectrum of the emitted positrons (red curve). Normalized energy dependence of the asymmetry positron emission (blue curve). Dashed line: weighted positron emission asymmetry $E(\varepsilon)a(\varepsilon)$. Note that for negative muons $a(\varepsilon)$ has the opposite sign.*

Since both the number of positrons and their decay asymmetry rise with energy, the asymmetry of the total angular distribution is mainly due to the high energy positrons.

If we integrate over all the energies (*i.e.* the ideal case where all the positrons are detected with similar efficiency), the average asymmetry is obtained with

$$\bar{A} = \int_0^1 a(\varepsilon) E(\varepsilon) d\varepsilon = \frac{1}{3} , \quad (1.16)$$

and we can write the angular distribution

$$d\Gamma = W(\theta) d\Omega = \frac{1}{4\pi\tau_\mu} \left(1 + \frac{1}{3} \cos \theta \right) d\Omega . \quad (1.17)$$

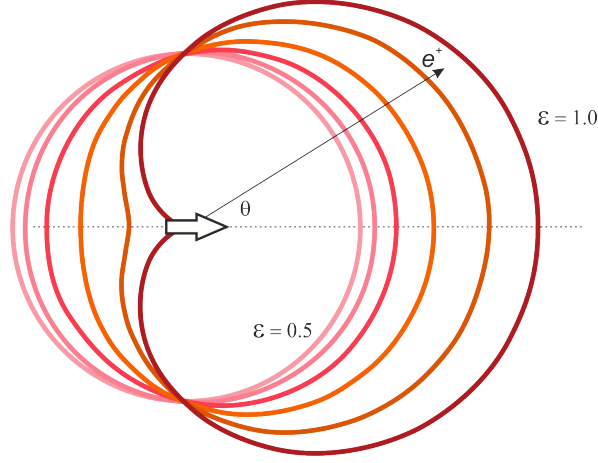


Figure 1.13.: Sketch of the anisotropic rate of positron emission as a function of the angle with the direction of the muon spin at decay time (cardioid curves). Energies between $\varepsilon = 0.5$ and $\varepsilon = 1.0$ are shown. For lower positron energies, the asymmetric rate becomes negative (see Fig 1.12).

1.5.3. Decay of a muon ensemble

μ SR experiments are based on the observation of the decay of an ensemble of say N_0 . As said, the decay is monitored through the observation of the emitted positrons. The number of positrons $N_{e^+}(t)$ which are emitted at time t is of course related to the number of muons decaying in the interval dt at time t . By looking at the full solid angle around the muons (assumed all located at the same place), we have:

$$N_{e^+}(t) = -\frac{dN_\mu}{dt} = \Gamma N_\mu(t) = \frac{1}{\tau_\mu} N_\mu(t) = \frac{1}{\tau_\mu} N_{\mu,0} e^{-\frac{t}{\tau_\mu}} . \quad (1.18)$$

$N_{e^+}(t)$ can be associated to the time evolution of the total activity during the “radioactive” decay of the implanted muons.⁶

If we now restrict ourselves to one direction of space, sustaining a solid angle $d\Omega$, we have (see Eq. 1.13):

$$N_{e^+}(t) = N_\mu(t) d\Gamma = \frac{N_{\mu,0}}{4\pi\tau_\mu} e^{-\frac{t}{\tau_\mu}} E(\varepsilon) [1 + a(\varepsilon) \cos \theta] d\varepsilon d\Omega . \quad (1.19)$$

We have here assumed that the muon ensemble is and remains completely polarized, *i.e.* $|\mathbf{P}(t)| = 1$. This is of course not the case in real life and the time evolution of $\mathbf{P}(t)$ is precisely what the μ SR technique is tracking (see Section 3). To obtain the real number of positrons observed by a detector, we have also to consider its energy efficiency and the solid angle $\Delta\Omega$ that it covers. A reduced energy efficiency will both reduce the number and the asymmetry of the observed positrons ($a(\varepsilon)$ and $E(\varepsilon)$ will be reduced), whereas a large solid angle will decrease the asymmetry (reducing \bar{A} , see Section 3) but will increase the number of the observed positrons by increasing the ratio $\Delta\Omega/(4\pi)$.

⁶This should not be mixed with the total number of remaining muons which is $N_\mu(t)$.

1.6. Muon magnetic moment and spin precession

1.6.1. Muon magnetic moment

Muons, as electrons and different elementary particles, have an intrinsic magnetic moment related to their spin (*i.e.* their intrinsic angular momentum)

The magnetic moment of the muon is

$$\mathbf{m}_\mu = \gamma_\mu \mathbf{I}_\mu = g_\mu \frac{e}{2m_\mu} \mathbf{I}_\mu \quad (1.20)$$

The gyromagnetic ratio γ_μ is the ratio of its magnetic moment (μ) to its spin (\mathbf{I}_μ) and is given as

$$\gamma_\mu = g_\mu \frac{e}{2m_\mu} . \quad (1.21)$$

The g -factor (which can be considered as the quantum mechanical correction with respect to the classical case) for the muon is predicted to be $g_\mu = 2$ by the Dirac equation, which describes spin-1/2 massive particles. In reality the present admitted value is $g_\mu = 2.0023318418$.⁷ By taking into account the value of the spin ($\frac{1}{2}\hbar$) we obtain for the muon magnetic moment

$$\begin{aligned} \mu &= g_\mu \frac{e}{2m_\mu} \frac{1}{2} \hbar = 4.490448 \times 10^{-26} \text{ J T}^{-1} \text{ or Am}^2 \text{ which is better expressed as} \\ &= 8.890597 \times \mu_N \\ &= g_\mu^* \times \mu_N \end{aligned} \quad (1.22)$$

Here $\mu_N = e\hbar/(2m_p)$ represents the magnetic moment of a Dirac particle possessing the mass and charge of the proton. It is the natural magnetic moment unit for particles like hadrons.⁸ Note that the g -factor g_μ is defined by calculating the magnetic moment with the real mass of the muon m_μ , whereas g_μ^* gives the value of the muon magnetic moment in μ_N . This is quite often mixed-up in literature (and probably in this script...).

The muon magnetic moment value is large (actually larger than the values observed for the nuclei) and therefore makes the muon a very sensitive probe to magnetic fields (in other words the interaction between a field and the moment will be large; see Eq. 1.27 in the next section).

⁷The very slight difference between the real value of g_μ and 2 (difference of the order of 0.1%) tells us that indeed the muon is an elementary particle. This difference is called the anomalous magnetic dipole moment and its value is important in precision tests of the QED theory (quantum electrodynamics) and for looking at effects beyond the Standard Model.

⁸Note that even though μ_N is expressed with the charge and mass of the proton, the real magnetic moment of the proton is much larger ($\mu_p = 2.792847 \times \mu_N$) reflecting the fact that the proton is not an elementary particle but is composed by 3 quarks.

1.6.2. Muon spin precession

When a magnetic field is sensed by the muon, its spin (or in other words, its magnetic moment) will precess due to the Larmor precession. We can understand the Larmor precession of the muon spin either classically or from a quantum mechanics point of view.

1.6.2.1. Classical view

Classically, a magnetic field \mathbf{B}_μ ⁹ will create a torque on the magnetic moment of the muon

$$\boldsymbol{\tau} = \boldsymbol{\mu} \times \mathbf{B}_\mu = \gamma_\mu \mathbf{I}_\mu \times \mathbf{B}_\mu , \quad (1.23)$$

where as we have seen γ_μ is the gyromagnetic ratio of the muon, *i.e.* the ratio of its magnetic moment ($\boldsymbol{\mu}$) to its spin (\mathbf{I}_μ). The torque can be expressed as the rate of change of the muon spin

$$\boldsymbol{\tau} = \frac{d\mathbf{I}_\mu}{dt} , \quad (1.24)$$

and therefore

$$\tau = \frac{\Delta I_\mu}{\Delta t} = \frac{I_\mu \sin \theta \Delta \phi}{\Delta t} = \gamma_\mu I_\mu B_\mu \sin \theta , \quad (1.25)$$

and by taking the derivative form we get the Larmor precession angular velocity

$$\omega_L = \gamma_\mu B_\mu . \quad (1.26)$$

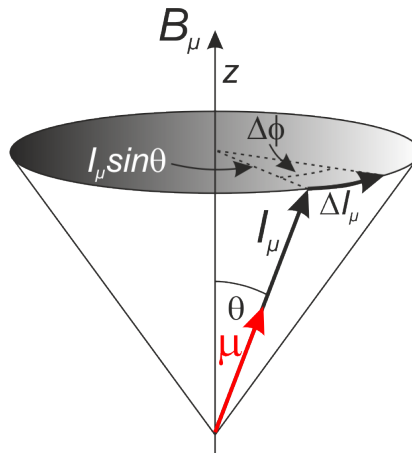


Figure 1.14.: *Classical view of the Larmor precession.*

⁹Per convention we will try to always call \mathbf{B}_μ the magnetic field sensed by the muon

1.6.2.2. Quantum mechanics view

For the quantum mechanics treatment we start from the Hamiltonian describing the interaction of the spin with the field

$$\mathcal{H} = -\boldsymbol{\mu} \cdot \mathbf{B}_\mu = -\gamma \mathbf{B}_\mu \cdot \mathbf{I}_\mu = -\gamma (B_x I_{\mu,x} + B_y I_{\mu,y} + B_z I_{\mu,z}) . \quad (1.27)$$

For example, if the field is along the z -axis we have the Hamiltonian

$$\mathcal{H} = -\gamma B_z I_{\mu,z} . \quad (1.28)$$

When looking at the time evolution of the spin state, we have to use the unitary operator¹⁰

$$\mathcal{U}(t, 0) = \exp\left(-\frac{i\mathcal{H}t}{\hbar}\right) , \quad (1.29)$$

which represents, when acting on a spin, a rotation by an angle $\gamma B_\mu t$ about the z -axis (given by the direction of the field). This can be seen when considering a muon spin pointing at $t = 0$ along the direction given by the angles (θ, ϕ) . Considering the quantization axis given by the field we can write¹¹

$$\Psi(\mathbf{r}, 0) = \cos \frac{\theta}{2} |+\rangle + \sin \frac{\theta}{2} e^{i\phi} |-\rangle . \quad (1.30)$$

The eigenvalues of the Hamiltonian acting on the states $|+\rangle$ and $|-\rangle$ are $-\gamma_\mu B_\mu \hbar/2$ and $\gamma_\mu B_\mu \hbar/2$, respectively.

We can write therefore

$$\begin{aligned} \Psi(\mathbf{r}, t) &= \mathcal{U}(t, 0) \Psi(\mathbf{r}, 0) \\ &= e^{-i\mathcal{H}t/\hbar} \left(\cos \frac{\theta}{2} |+\rangle + \sin \frac{\theta}{2} e^{i\phi} |-\rangle \right) \\ &= \cos \frac{\theta}{2} e^{+i\gamma_\mu B_\mu t/2} |+\rangle + \sin \frac{\theta}{2} e^{i\phi} e^{-i\gamma_\mu B_\mu t/2} |-\rangle \\ &= e^{+i\gamma_\mu B_\mu t/2} \left(\cos \frac{\theta}{2} |+\rangle + \sin \frac{\theta}{2} e^{i(\phi - \gamma_\mu B_\mu t)} |-\rangle \right) \end{aligned} \quad (1.31)$$

Comparing with the state at time $t = 0$ (and recalling that an overall phase is not relevant in quantum mechanics), we see that the new spin state corresponds to change of the azimuthal angle of $\gamma_\mu B_\mu t$, corresponding to a Larmor angle velocity of

$$\omega_L = \gamma_\mu B_\mu , \quad (1.32)$$

as in the classical case.

As already seen, the value of the muon magnetic moment, and therefore of the gyro-magnetic ratio, is large. This leads to large Larmor frequencies of the muon of $\nu_\mu = 135.538817 \text{ MHz/T}$ (see Table 1.2).

¹⁰See the nonrelativistic time-dependent Schrödinger equation

$$i\hbar \frac{\partial}{\partial t} \Psi(\mathbf{r}, t) = \mathcal{H} \Psi(\mathbf{r}, t)$$

¹¹Remember that the muon is a spin 1/2 particle. General superposition state \rightarrow see Bloch sphere.

1.7. Atmospheric muons

Most muons observed at the surface of the Earth are produced by primary cosmic rays in the upper atmosphere. They are the most numerous energetic particles arriving at sea level, with a flux of about 1 muon per square centimeter per second. This can be compared to a solar neutrino flux of about $5 \times 10^6 \text{ cm}^{-2}\text{s}^{-1}$.

The mean energy of muons reaching sea level is about 4 GeV. Muons, being charged particles, interact with matter by ionizing it. The loss of energy by muons passing through the atmosphere is proportional to the amount of matter they traverse. The medium is usually characterized by its density (g/cm^3) times the distance traveled in centimeters. This is sometimes called the “interaction length” and is measured in g/cm^2 . The energy loss for muons is about 2 MeV per g/cm^2 (see Fig. 2.5). The interaction depth of the atmosphere is about 1000 g/cm^2 , so muons lose about 2 GeV in passing through the atmosphere (see Exercises for a slightly better approximation of the interaction length). With the sea level mean energy of muons detected at the surface equal to 4 GeV, this suggests an original muon energy in the neighborhood of 6 GeV.

Most muons are thought to be created at altitudes of about 15000 meters and travel with other particles to the Earth in conical showers within about 1 degree of the trajectory of the primary particle which creates them. Measurement of muon flux at different altitudes is a useful example of relativistic time dilation. With an energy of 4 GeV, the time dilation factor is $\gamma = 38.8$.

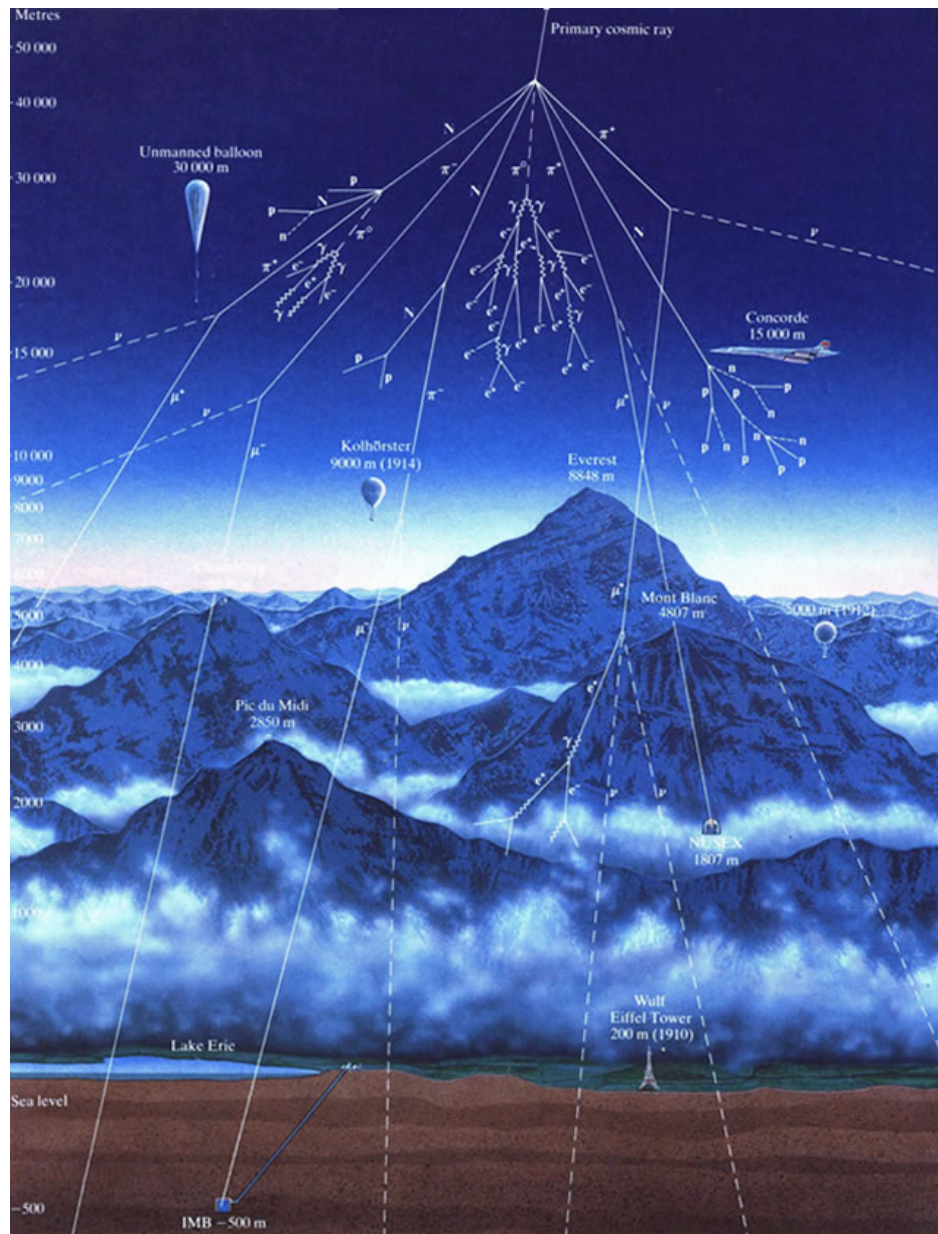


Figure 1.15.: Schematic view of the particle shower produced by cosmic rays.

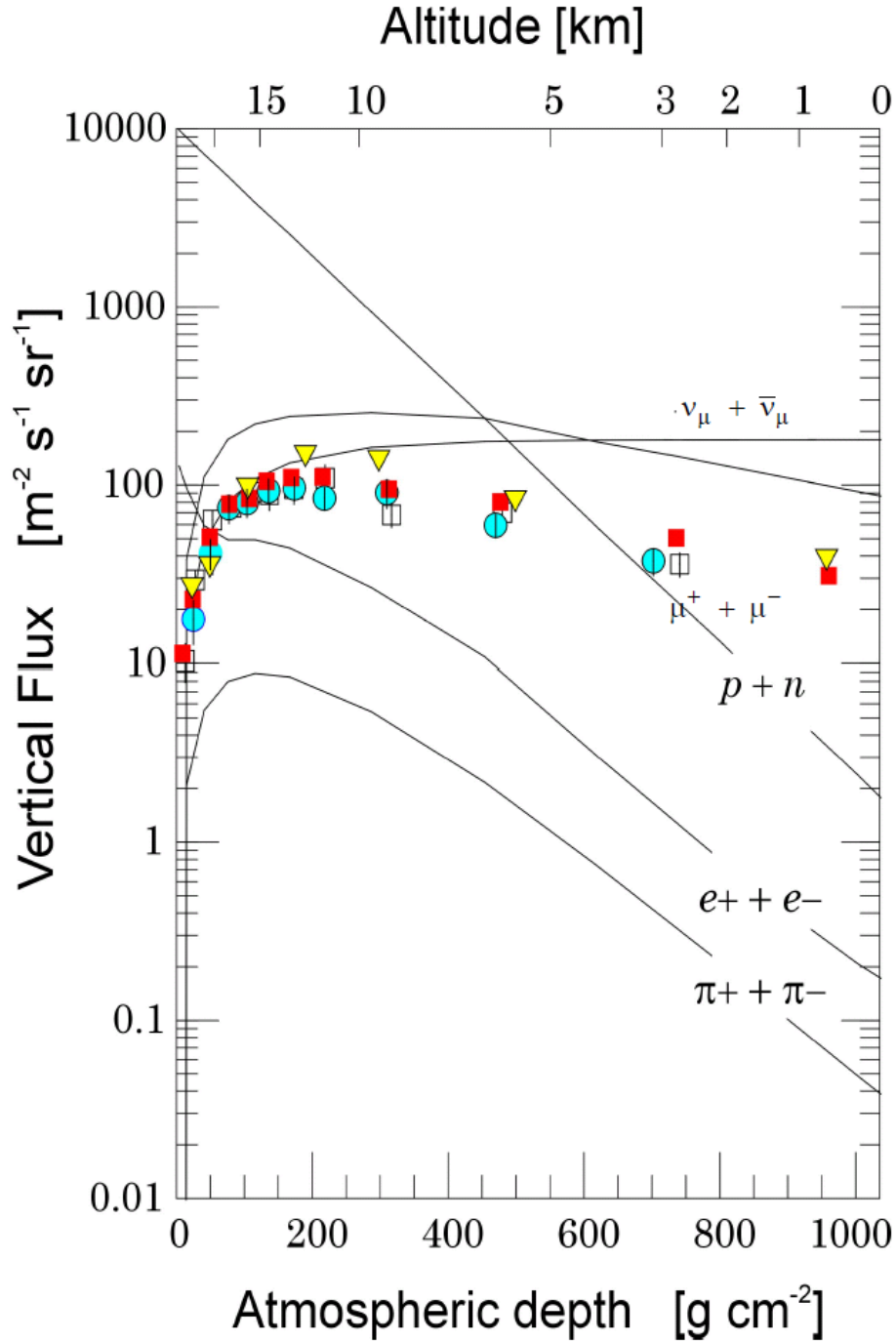


Figure 1.16.: *Cosmic rays flux.*

Even though atmospheric muons cannot be used to performed muon-spin spectroscopy experiments, they can be used to make radiography from large massive objects. Some projects in Japan were dedicated to the observation of the magma inside of a spent volcano. Another very recent and very much publicized example is the discovery of a large cavity in the Cheops's (Khufu's) pyramid [20]. In this experiment huge muon detectors were installed at the base of the pyramid. Absorption measurements were performed. In such measurements, a variation of muon counts would reveal a change in the pyramid density, in other word an

excess of muons would reveal the presence of a cavity in the pyramid.

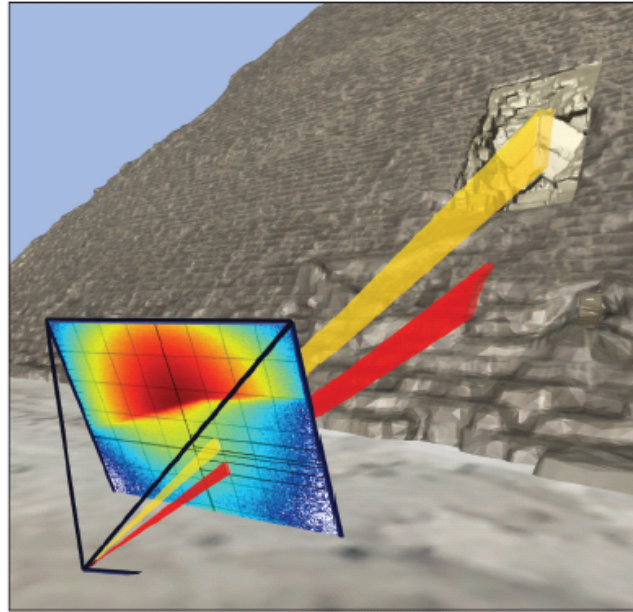


Figure 1.17.: Sketch of the muon detector. On the two cones excess of muons were observed (see also Fig. 1.18 and 1.19).

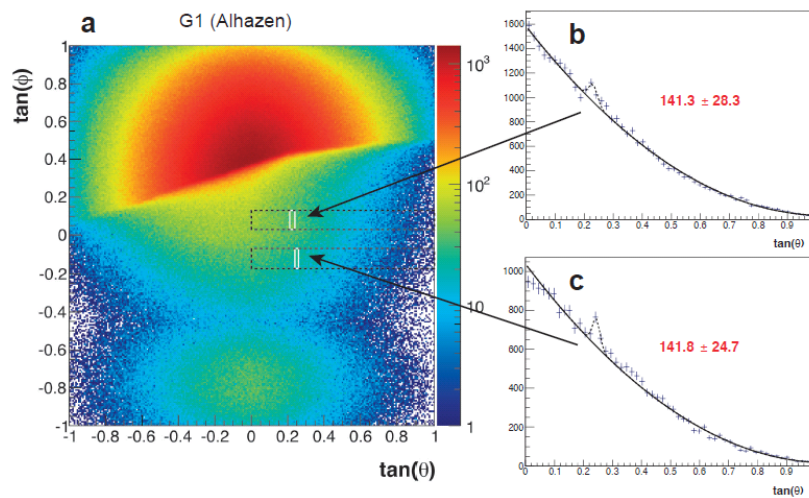


Figure 1.18.: Two regions with excess of muons were observed. The lower one represents the known Grand Gallery. The upper one represents an unknown cavity (see also Fig. 1.19).

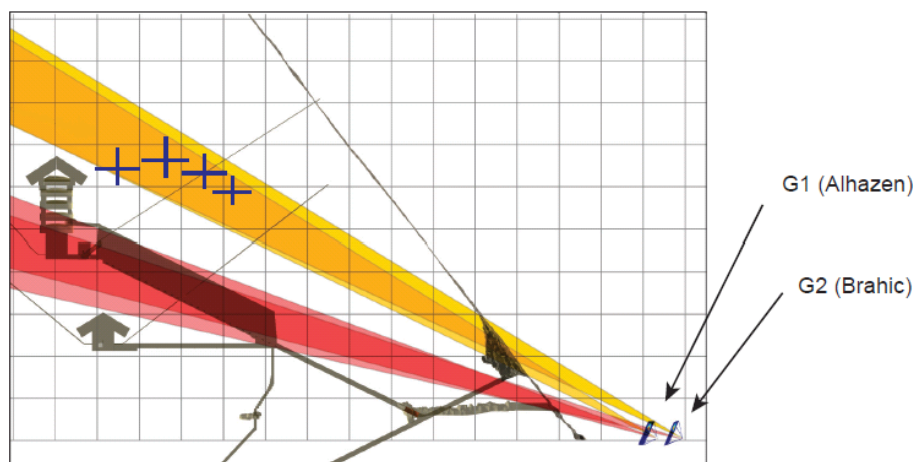


Figure 1.19.: *Schematics of the position of the unknown cavity.*

Recently, TEPCO (Tokyo Electric Power Company) has begun to investigate its damaged nuclear reactor in Fukushima using cosmic rays. Here a combination of absorption and scattering experiments are being followed.

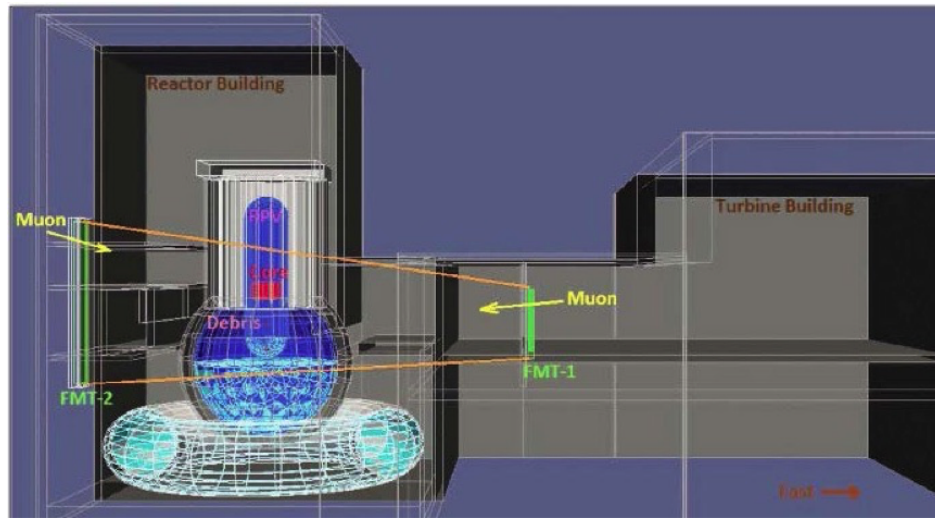


Figure 1.20.: Schematics of one Fukushima reactor with muon detectors.

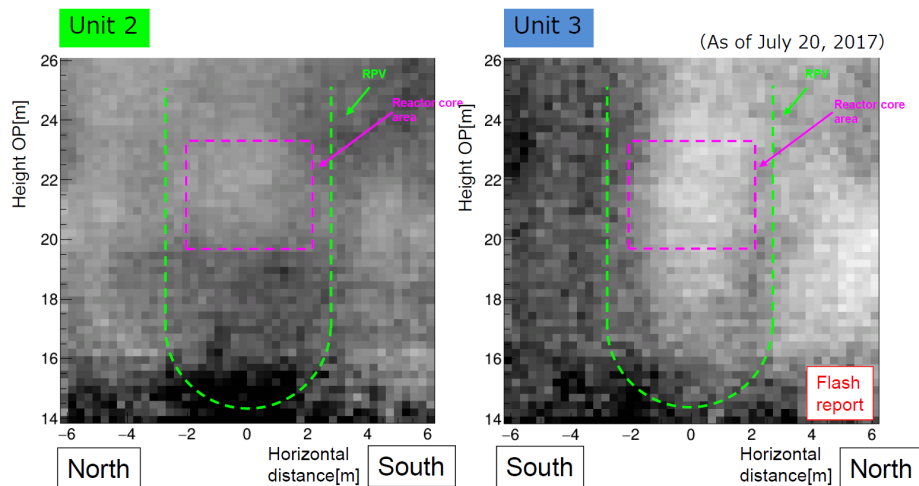


Figure 1.21.: Comparisons between measurements performed for the Reactors 2 and 3. Whereas indications are present that fuel is located in the Reactor Pressure Vessel (RPV) for the unit 2, no indication of spent fuel is so far observed for the unit 3.

1.8. “Man-made” muons

The muons created in the high atmosphere have too high energy and are too few to be reasonably used for condensed matter experiments. Therefore, muon spin-spectroscopy experiments are solely possible using high-energy accelerators where polarized muon beams of high intensity are available.

In the next Sections we will first describe different types of accelerators to produce pions, the parent particle of the muon. We will then see different muon beams characterized by different energies. Note that the production description of the so-called Low-Energy Muons (with energies of the order keV) will be presented in the Section 7.

Here, in addition to the high-energy and surface muon beams, we will also look at the typical devices located on a beamline which will transport the beam to the experiment.

1.8.1. Pion production: 3 different possible accelerators

In addition to the pions produced in the atmosphere, linear accelerators (linacs), cyclotrons, and synchrotrons are three ways to accelerate protons to eventually produce pions.

As their name suggests, linacs accelerate particles in a straight line. The particles travel in a pipe-shaped vacuum chamber. Electrodes inside the pipe are spaced so that a driving radio frequency can be timed to energize them as particles are in the gap between electrodes, and thereby accelerate them as they travel from one gap to another.

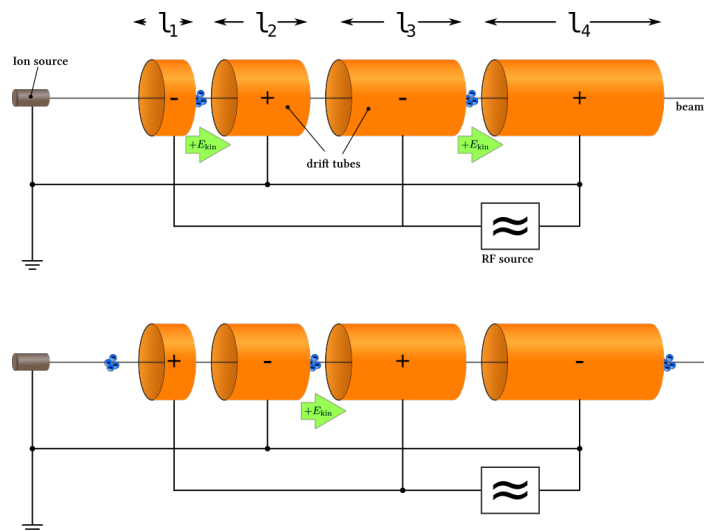


Figure 1.22.: Schema of a linear accelerator.

(Taken from https://en.wikipedia.org/wiki/Linear_particle_accelerator).

Cyclotrons accelerate particles along a spiral path and are held in that path by a static electromagnetic field perpendicular to the spiral path. The protons are injected into the center of

the cyclotron into a vacuum chamber between two hollow metal electrodes (because of the resemblance of this semicircular structure with the capital D, the electrodes have been called “dees”). An alternating RF voltage is applied to one dee and then the other. The timing of the RF voltage is switched between dees, accelerating the particles and increasing the diameter of their circular path with every revolution, turning it into a spiral. The RF frequency is of the order of tens of MHz and therefore finally leading to quasi-continuous muon beams (see below).

A cyclotron can accelerate protons to energies no greater than 25 MeV. This limitation is imposed by the relativistic increase in the proton mass as its speed approaches that of light. As the mass increases, the orbital frequency decreases, and the particles cross the gap at times when the electric field decelerates them. To overcome this limitation, a technique is to strengthen the magnetic field near the periphery of the dees, hence keeping the angular velocity $\omega_c = eB/\gamma m$ constant¹². Cyclotrons operated in this way are called *isochronous*. Such isochronous cyclotrons can produce beams with energy up to about 1 GeV. The limitation is due to the magnetic field limitation (saturation field of about 2 T). Another technique is to effectively change the frequency of the RF voltage (reducing the frequency when the mass of the proton increases with energy at large radius). Cyclotrons operated in this way are called *synchrocyclotron*. However the disadvantage of a synchrocyclotron is the production of a pulsed beam with relatively low intensity.

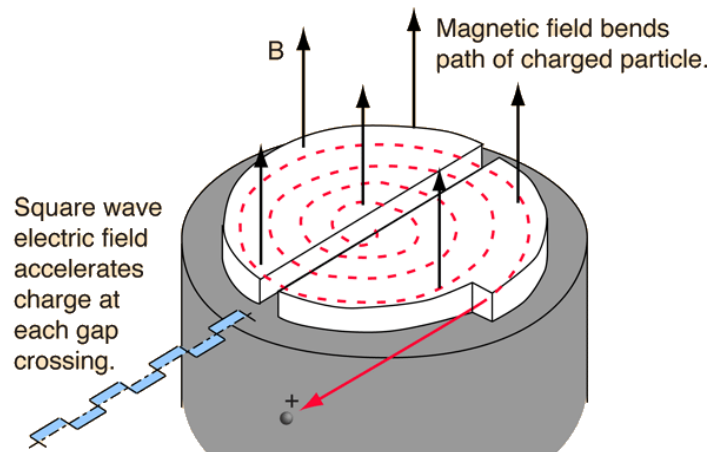


Figure 1.23.: Cyclotron: operation principle.

(Taken from <http://hyperphysics.phy-astr.gsu.edu/hbase/magnetic/cyclot.html>).

Finally, synchrotrons, like cyclotrons, are cyclic accelerators and send particles into a closed-loop path. Acceleration is achieved by the application of radio frequency electric fields at RF cavities along the circumference of the ring. Unlike cyclotrons, the synchrotron's loop is not a spiral and therefore the magnetic fields bending the proton trajectory must be increased synchronously with the acceleration in order to keep the particles on the constant radius path. The path can be a circle, oval or a polygon with rounded corners. Synchrotrons produce pulsed proton beams which can reach very high energy (up to TeV). The typical

¹²In the classical limit the principle of a cyclotron is expressed by equating the centrifugal force to the Lorentz force, i.e.: $evB = mv^2/r$, and therefore $\omega_c = v/r = eB/m$.

pulse frequency is 50 Hz. Due to the closed-path shape, a synchrotron needs an injection accelerator (usually a linac system).

1.8.2. Pion production: for example at the Paul Scherrer Institute

At the Paul Scherrer Institute (PSI, Villigen, Switzerland), protons are first extracted from a source made up of hydrogen atoms and then accelerated in three steps.

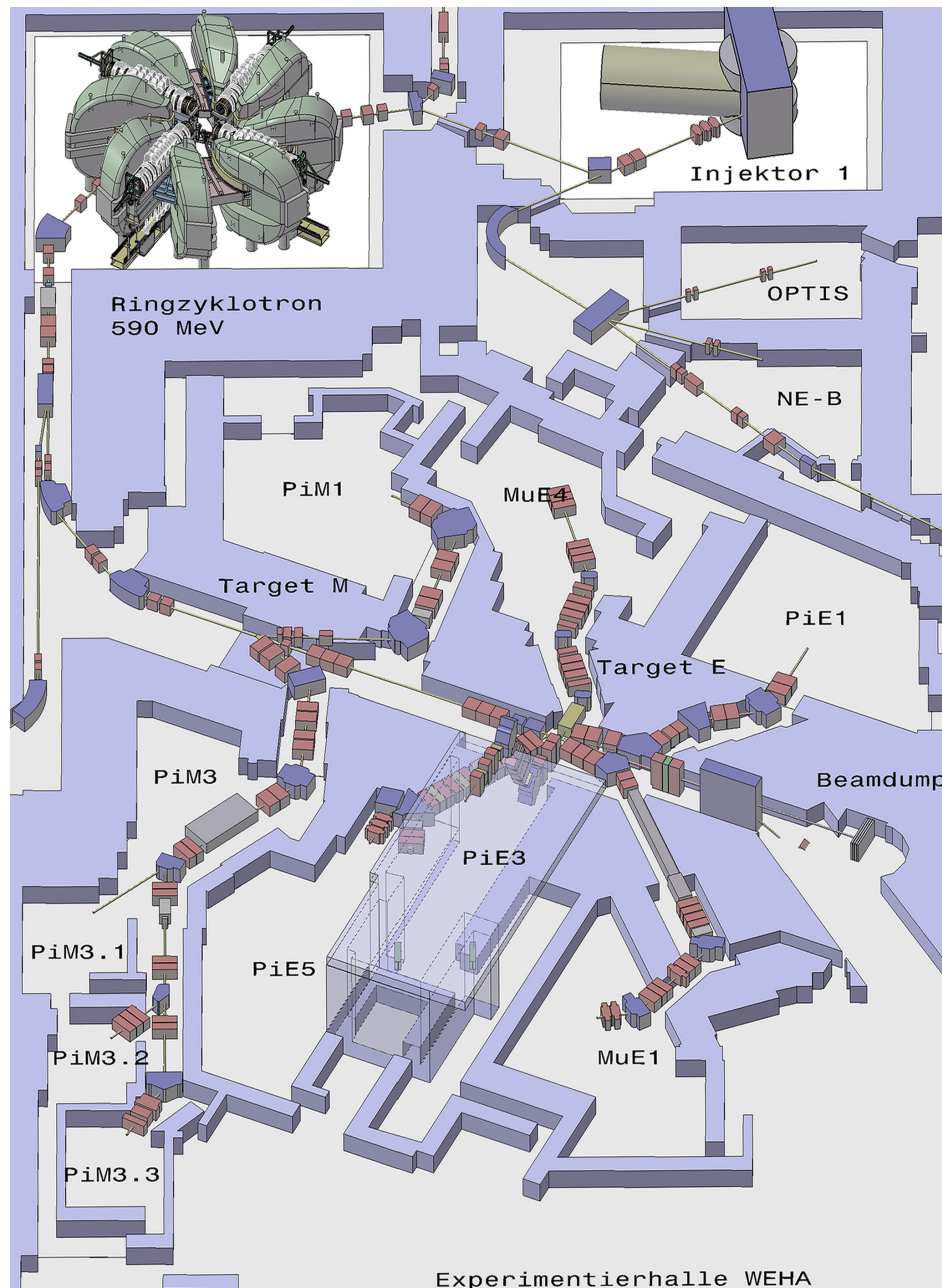


Figure 1.24.: Sketch of the High Energy Proton Accelerator (HIPA) at PSI (Courtesy PSI).

- A Cockcroft-Walton accelerator, which actually also contains the proton source, is used as the first stage from which protons are fed into Injector II (both not shown on Fig. 1.24).



Figure 1.25.: *PSI Cockcroft-Walton accelerator.*

- The Injector II is a first pre-accelerator, actually a small ring cyclotron. It accelerates protons to a speed of approximately 37% of the speed of light (72 MeV) before feeding them to the center of the large ring cyclotron.
- The core of this facility is the large ring isochronous cyclotron with a diameter of approximately 15 meters, in which protons are accelerated to their terminal speed of almost 80% of the speed of light over 186 revolutions (equivalent to a kinetic energy of 590 MeV).

As mentioned above, in a cyclotron the protons are accelerated in stages, with the electrical fields building up every time particles pass through an accelerator cavity and giving them an additional impulse. At PSI, several accelerator cavities of this kind are positioned between the magnets in the path of the beam. The principle components of the large PSI ring cyclotron are eight sector magnets and four accelerator cavities.

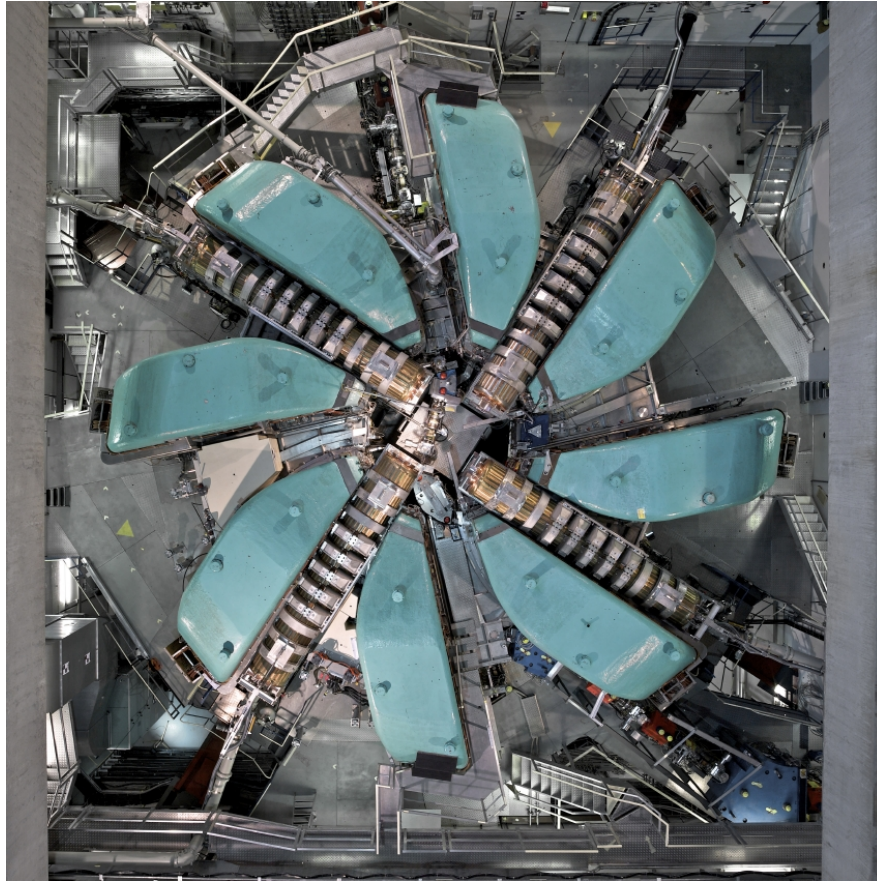


Figure 1.26.: *The PSI 590 MeV cyclotron.*

After the acceleration, the protons are transported in the so-called proton-channel toward two graphite production targets into which the pions are produced:

- The first target is rather thin with a thickness of 5 mm. It is called the target M: (“Mince” – in French),
- The second one is rather thick and is available in two versions with a thickness of either 4 or 6 cm. It is called the target E: (“Epaisse” – in French). Figures 1.27 and Figures 1.28 represent the target E and the proton beam trajectory.

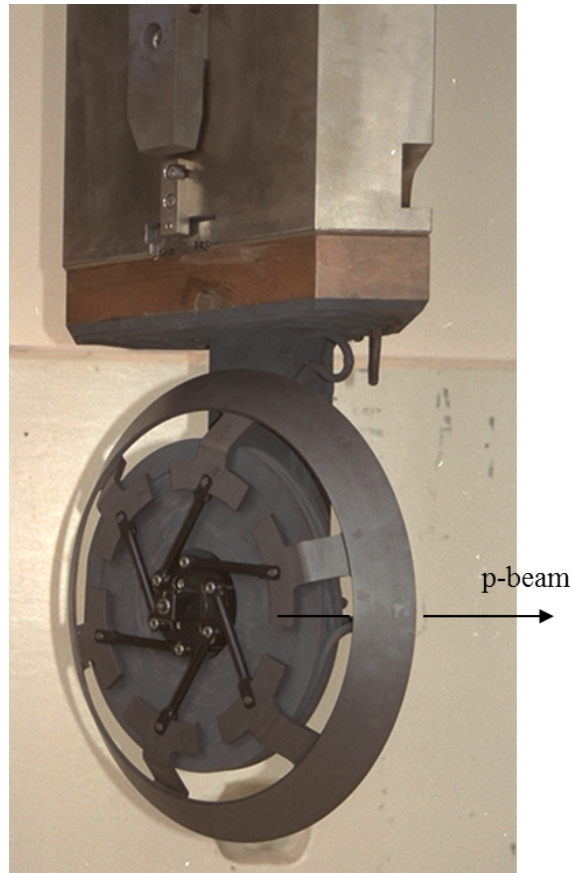


Figure 1.27.: Photograph of the PSI E graphite target.

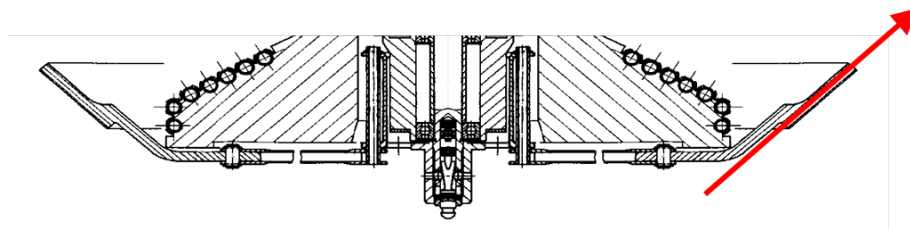


Figure 1.28.: Schematic of the PSI E target (top-view). The red arrow indicates the direction of the proton beam. After the target, the beam is transported to the neutron spallation source SINQ or to the beam dump.

Rough estimate of the number of pions produced in the E target:

- PSI cyclotron current: $I = 2200 \mu\text{A} = 1.373 \times 10^{16}$ protons/s (as $+e = 1.602 \times 10^{-19}$ C).
- The cross section is roughly $2 \text{ fm}^2 = 2 \times 10^{-30} \text{ m}^2$ (see Fig. 1.7).
- The number of mole of graphite per cm^3 is given by $n = \rho/(4A)$, where $\rho = 2.23 \text{ g/cm}^3$ is the graphite density and $A = 12$ is the mass number of carbon. The

factor 4 arises as 4 C atoms are in the unit cell.

The number of carbon atoms per cm^3 is given by $n_C = n 4 N_{\text{Av}}$, where N_{Av} is the Avogadro number. Here again the factor 4 arises as 4 carbon atoms are in the unit cell.

- Assuming a constant cross section σ of the reaction proton-nucleon through the target, the total cross section as seen by a proton will be $\sigma_{\text{tot}} = n_C V \sigma = n_C S_{\text{tot}} d \sigma$, where $V = S_{\text{tot}} d$ is the volume of the target (with S_{tot} the surface of the target and d the length of the target, say 4 cm). For one proton, the probability to have a collision with a nucleon is $\sigma_{\text{tot}}/S_{\text{tot}} = n_C \sigma d$.
- Therefore the number of pions produced will be $I n_C \sigma d \approx 1.2 \times 10^{14}$ pions/s over the entire 4π solid angle.

1.8.3. Muon beams for condensed matter

1.8.3.1. “High-energy” muons

For some experiments, one needs muons with a high energy (*i.e.* bigger than the 4.1 MeV that they have in the pion reference frame). This can be necessary if the sample is placed in a container with thick walls (for example in the case of a liquid or for a sample place inside a clamp pressure cell). The solution to obtain high-energy muons is to first extract high energy pions from the production target. These pions are first selected by a bending magnet (where pion of a given momentum will have the correct trajectory) and are transported to a long superconducting solenoid (“decay muon channel”) where the pions decay in flight.

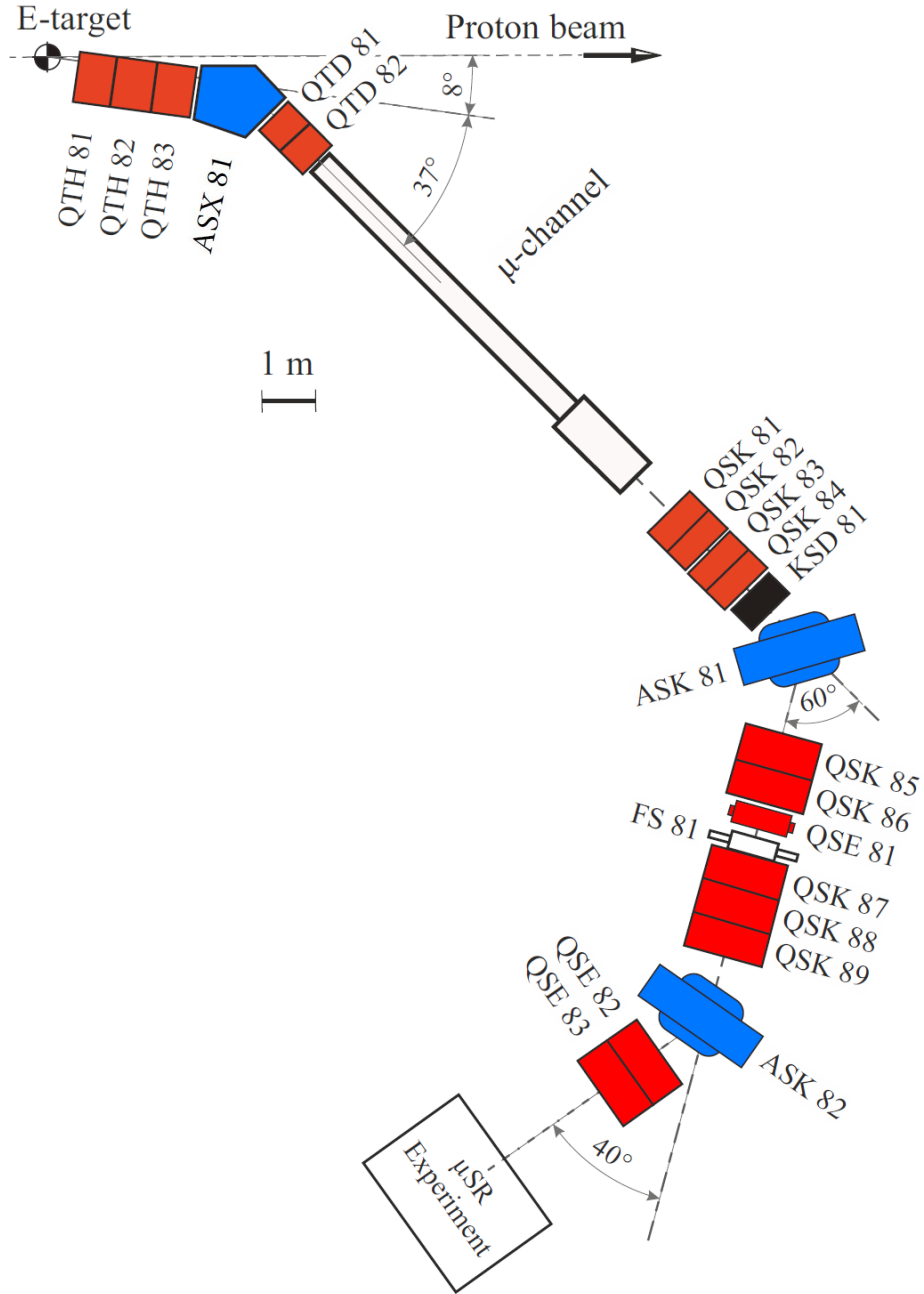


Figure 1.29.: Schematic view of the μ E1 high energy beamline at PSI.

Depending on the muon direction emission, resulting muons beams with different polarization can be obtained.

In practice, two extreme conditions are used:

1. The muon is emitted in the direction of the pion momentum, *i.e.* “forward” direction. The momenta \mathbf{p}_μ^0 (corresponding to the muon momentum in the pion reference frame) and \mathbf{p}_π are additive and the final muon momentum \mathbf{p}_μ is greater than the one of the pion. The muon has a spin pointing in the opposite direction of its propagation.

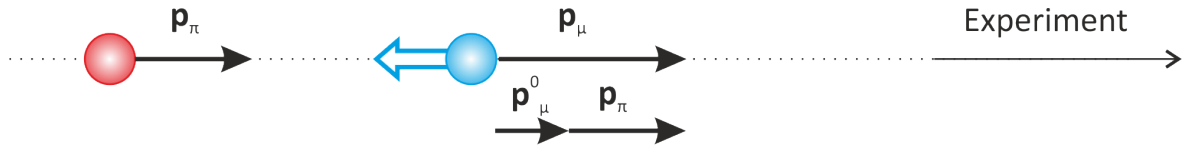


Figure 1.30.: Schematic view of the creation of “forward” muons in the muon decay channel.

2. The muon is emitted in the direction of the pion momentum, *i.e.* “backward” direction. The momenta \mathbf{p}_μ^0 (corresponding to the muon momentum in the pion reference frame) and \mathbf{p}_π are pointing in opposite directions and the final muon momentum \mathbf{p}_μ is smaller than than the one of the pion. The muon has a spin pointing in the direction of its propagation.

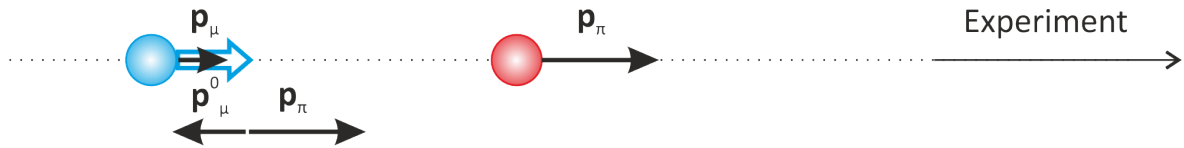


Figure 1.31.: Schematic view of the creation of “backward” muons in the muon decay channel.

The choice between these two extreme cases is performed by tuning the first bending magnet (momentum selection) after the decay channel (magnet ASK81 shown in Fig. 1.29).

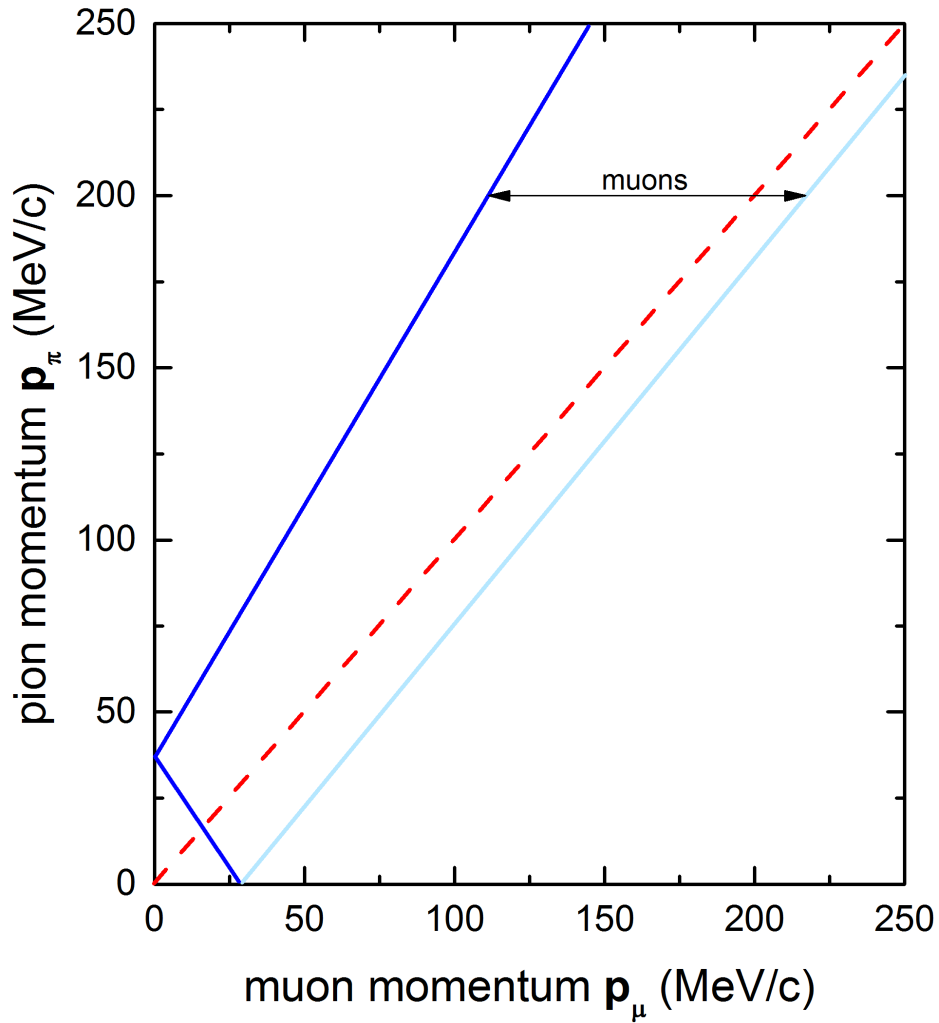


Figure 1.32.: Decay kinematics of the pion decay. The red curve would correspond to muons with a momentum equal to the one of the pions. The allowed region is located in-between the “forward” muons (light blue) and the “backward” muons (dark blue).

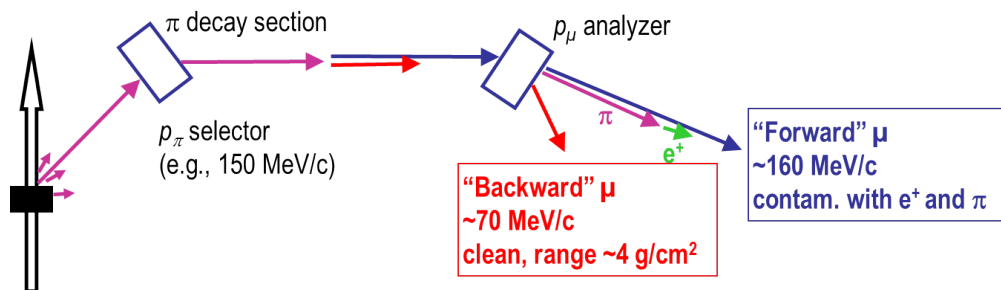


Figure 1.33.: Principle of a high energy beamline (as $\mu E1$ at PSI). In practice “backward” muon beams are used which are less energetics but are much less contaminated by other particles. For high-pressure experiments, one usually use momentum up to 110 MeV/c.

1.8.3.2. “Surface” muons

The large majority of the muon beamlines around the world are so-called “surface” or “Arizona” beam (recalling the pioneer works of Pifer *et al.* from the University of Arizona [21]). The fundamental difference with a high-energy beam is that here muons are extracted from the production target. These muons arise from pion decaying at rest still inside, but near the surface, of the production target.¹³ As already seen, the muons arising from pions decaying at rest are 100% polarized, ideally monochromatic and have a low momentum of 29.8 MeV/c and have a range width in matter of the order of 130 mg/cm² (see Section 2.2.1). Hence the paramount advantage of this type of beam is the possibility to use relatively thin samples.

Another advantage is that they are rather easy to be manipulated, as for example concerning their polarization or their detection.

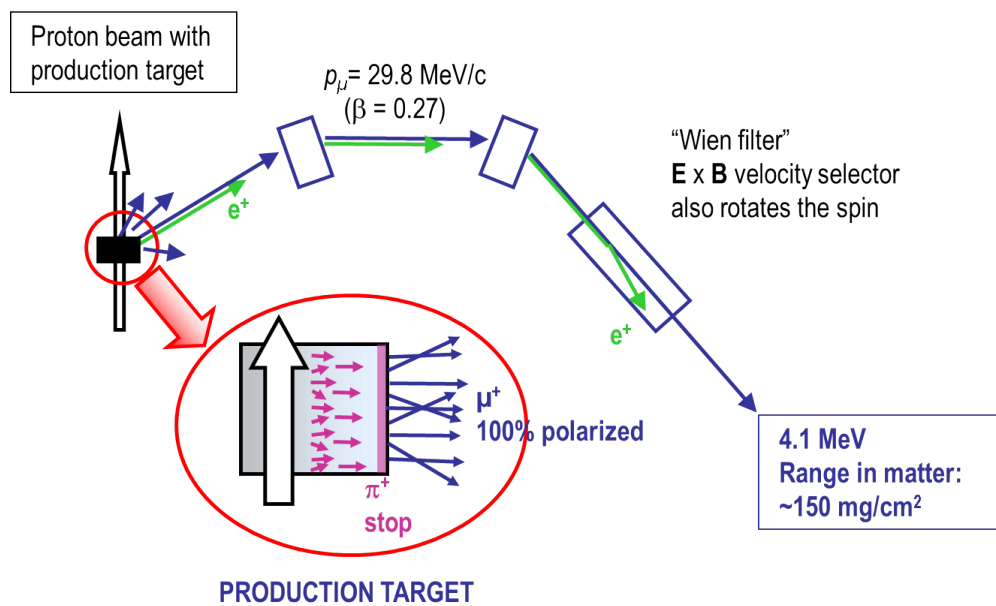


Figure 1.34.: Principle of a surface muon beamline (as $\pi E3$ or $\pi M3$ at PSI).

¹³Pions decaying deep inside the target will produce muons which will not have enough energy to escape the target (see Section 2).



Figure 1.35.: *Picture of the surface muon beamline $\pi M3$ at PSI.*

1.8.3.3. Few words about a typical beamline and beam optics

The beam optics can be defined as the whole process of guiding a charged particle beam from A to B. This is usually done with magnets. The point A is usually the source and B the experiment.

As seen in Section 1.3.3, after a pion decay, the muon has a well defined spin polarization with respect to its velocity. However, the velocity direction is changed (through bending magnets) in a beamline. One can therefore ask himself how come the polarization is maintained during the muon transport?

As seen above (Section 1.8.1), the muon cyclotron angular velocity ω_c (describing the change of the trajectory in field) is given by:

$$\omega_c = \frac{eB}{m} . \quad (1.33)$$

On the other hand the Larmor angular velocity ω_L is given by (see Sections 1.6.2 and 3.2.2):

$$\omega_L = \gamma_\mu B = g_\mu \frac{e}{2m_\mu} B \simeq \frac{eB}{m} . \quad (1.34)$$

This results to the fact that the cyclotron frequency is identical to the Larmor frequency and therefore a bending of the muon trajectory by a magnetic field will be accompanied by a spin direction rotation such that the muon-spin direction will always stay exactly opposite to the muon momentum. This is of paramount importance when transporting the muons from the production target to the experimental area.

Two types of magnets are used for the transport: bending magnets (dipoles) and focusing magnets (quadrupoles).

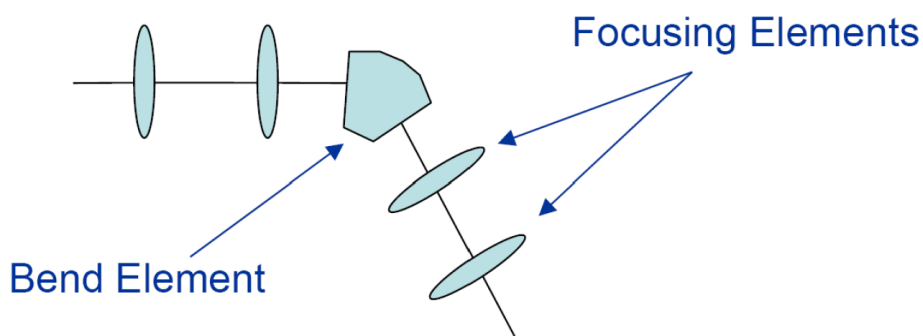


Figure 1.36.: Schematic view of the typical elements on a beamline.

1.8.3.3.1. Dipole magnets A dipole magnet provides a constant field \mathbf{B} . The field lines in a magnet run from North to South pole (see Fig. 1.37).

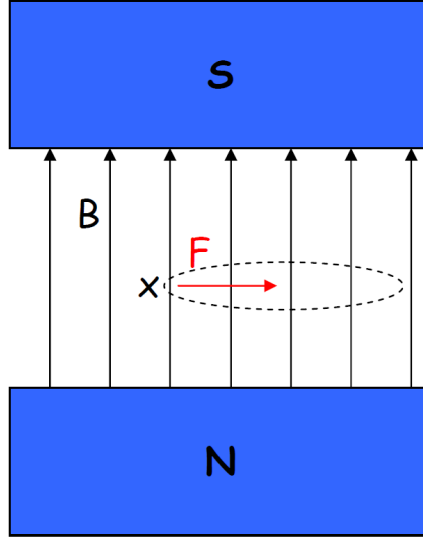


Figure 1.37.: Schematic view of the field in a dipole magnet. The force acting on muons flying into the paper is shown.

Recall the Lorentz Force on a particle:

$$F = ma = e |(\mathbf{E} + \mathbf{v} \times \mathbf{B})| = \frac{mv^2}{r} , \quad (1.35)$$

where $m = \gamma m_0$ is the relativistic mass and r is the bending radius. In the absence of an electrical field and considering that \mathbf{B} and \mathbf{v} are perpendicular (particles flying into the page at the point \times in Fig. 1.37), one obtains

$$\frac{1}{r} = \frac{e B}{p} . \quad (1.36)$$

And numerically:

$$\frac{1}{r} [\text{m}^{-1}] = 0.2998 \frac{B [\text{T}]}{p [\text{GeV}/c]} . \quad (1.37)$$

Therefore, for a given bending radius (given by the geometry of the beamline), by tuning the field one tunes the momentum of the particle flying with the correct trajectory. Therefore the first bending magnet along a beamline will select the momentum of the beam.¹⁴

¹⁴Keep in mind that here solely the momentum is selected and that different particles (with obviously different velocities) can possess the same momentum. To “clean” the beam a Wien filter is required (see below).

A sector mass spectrometer uses the same principle but, prior to the bending by the main field, a velocity selection is performed by the combined action of perpendicular electric and magnetic fields *i.e.* this corresponds to the Wien filter that we apply here after the bending.

1.8.3.3.2. Quadrupole magnets To focus the beam, so-called “quadrupole magnets” are used. They consist of groups of four magnets designed in such a way that the lowest significant terms in the field equations are quadrupole. They produce a magnetic field whose magnitude grows as a function of the distance from beam center axis.

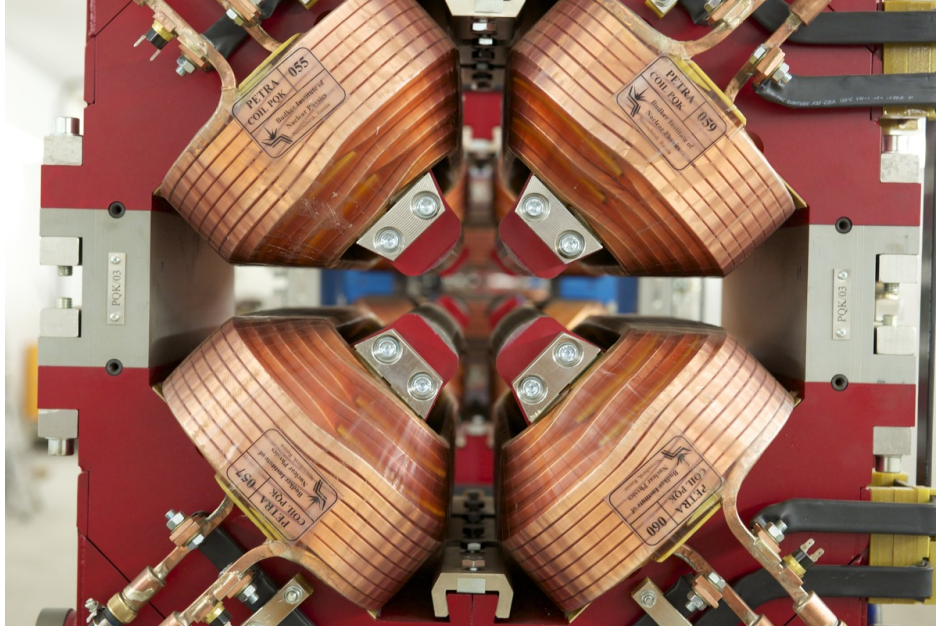


Figure 1.38.: Typical quadrupole magnet.

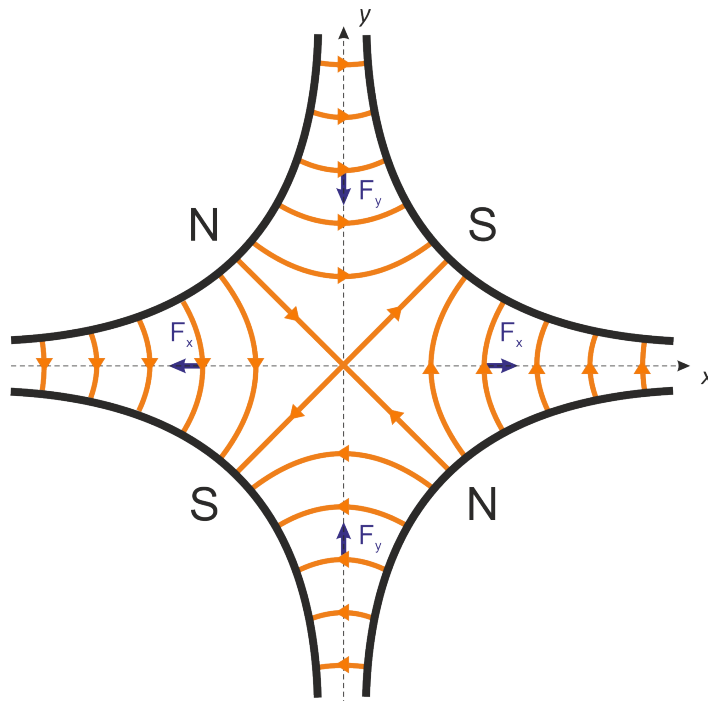


Figure 1.39.: Schematic of the magnetic fields in a quadrupole magnets (orange lines). The pole shoes have the shape of hyperbolas. The forces are represented for muons flying into the paper.

Between the pole shoes, we do not have any electrical currents and one can write using the Maxwell equations:

$$\nabla \cdot \mathbf{B} = 0 \quad (1.38)$$

$$\nabla \times \mathbf{B} = 0 \quad (1.39)$$

From the first equation, there exists a vector potential \mathbf{A} , such that $\mathbf{B} = \nabla \times \mathbf{A}$ and from the second one, there exists a scalar potential $\mathbf{B} = -\nabla\Phi$. By taking the long cylinder approximation, the component of the field along the beam is vanishing, *i.e.* $B_z = 0$ and $\mathbf{A} = (0, 0, A)$. One can therefore write that:

$$B_x = \frac{\partial A}{\partial y} = -\frac{\partial \Phi}{\partial x} \quad (1.40)$$

$$B_y = -\frac{\partial A}{\partial x} = -\frac{\partial \Phi}{\partial y} \quad (1.41)$$

One can show that a magnetic field $\mathbf{B} = (B_x, B_y, B_z)$ with B_z constant (in our case equal to zero) and B_x, B_y given by

$$B_y + i B_x = C_n (x + i y)^{n-1} , \quad (1.42)$$

(where C_n is a complex constant) satisfies Eqs 1.38 and 1.39.¹⁵

Fields of the form given by Eq. 1.42 are known as “multipole” fields, with the index n indicating the order of the multipole.¹⁶

One can use the principle of superposition and add a set of multipole fields to obtain a general magnetic field:

$$B_y + i B_x = \sum_{n=1}^{\infty} C_n (x + i y)^{n-1} . \quad (1.43)$$

The coefficients C_n characterize the strength and orientation of each multipole component. Using the polar coordinates ($x = r \cos \theta$ and $y = r \sin \theta$), we have

$$B_y + i B_x = \sum_{n=1}^{\infty} C_n r^{n-1} e^{i(n-1)\theta} . \quad (1.44)$$

We see that the strength of the field in a pure multipole of the order n varies as r^{n-1} with distance from the magnetic axis¹⁷. If we express the field in the polar components ($B_x = B_r \cos \theta - B_\theta \sin \theta$ and $B_y = B_r \sin \theta + B_\theta \cos \theta$) we have

$$B_\theta + i B_r = \sum_{n=1}^{\infty} C_n r^{n-1} e^{in\theta} . \quad (1.45)$$

¹⁵This is seen by applying the differential operator $\partial/\partial x + i\partial/\partial y$ to each side of the Eq. 1.42.

¹⁶ $n = 1$ is a dipole field, $n = 2$ is a quadrupole field, $n = 3$ is a sextupole field and so on.

¹⁷A “pure” multipole represents the case where only one value of either b_n or a_n is different from zero, whereas all the other coefficients are equal to zero.

Therefore, for a pure multipole of order n , rotation of the magnet through π/n around the z axis simply changes the sign of the field as actually shown on Fig. 1.39 ($n = 2$) and Fig 1.37 ($n = 1$).

The constants C_n have units which depend on the order of the multipole. For a dipole, the unit of C_1 (dipole) is tesla (T); for a quadrupole, the unit of C_2 is T/m; for a sextupole, the unit of C_3 is T/m², and so on. But, the multipole components are usually given in dimensionless units. In that case, a reference field, B_0 , and a reference radius, R_0 are given. They can be chosen arbitrarily, but must be specified if the C_n coefficients need to be fully interpreted.

By writing the constant C_n as

$$C_n = \frac{B_0}{R_0^{n-1}} (b_n + i a_n) , \quad (1.46)$$

then Eq. 1.43 can be expressed as

$$B_y + i B_x = B_0 \sum_{n=1}^{\infty} (b_n + i a_n) \left(\frac{x + i y}{R_0} \right)^{n-1} . \quad (1.47)$$

One can see that the coefficient a_n and b_n will determine the orientation of the field. As a convention, a pure multipole is called a “normal” multipole if $b_n \neq 0$ and $a_n = 0$, whereas if $a_n \neq 0$ and $b_n = 0$ it is called a “skew” multipole. These coefficient are related to the derivatives of the field:

$$\frac{\partial^{n-1} B_y}{\partial x^{n-1}} = (n-1)! \frac{B_0}{R_0^{n-1}} b_n \quad \text{and} \quad (1.48)$$

$$\frac{\partial^{n-1} B_x}{\partial y^{n-1}} = (n-1)! \frac{B_0}{R_0^{n-1}} a_n . \quad (1.49)$$

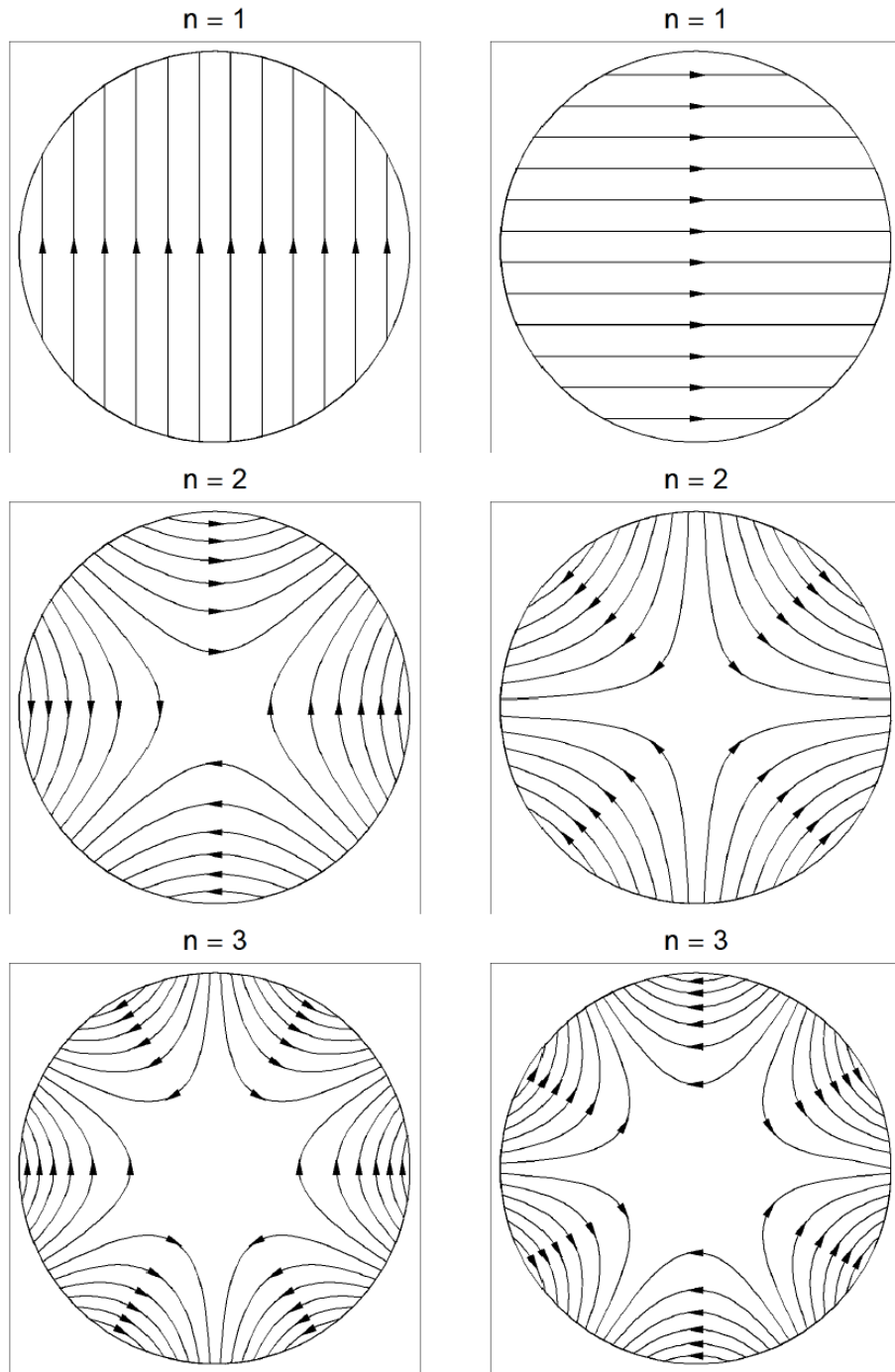


Figure 1.40.: “Pure” multipole fields. Top: dipole. Middle: quadrupole. Bottom: sextupole. Fields on the left are “normal”; those on the right are “skew”.

We see that the fields shown on Fig 1.37 and Fig. 1.39 correspond to “pure” dipole and quadrupole (in these case “normal” fields), respectively.

The field for the quadrupole is given by

$$B_x = gy \quad (1.50)$$

$$B_y = gx \text{ with} \quad (1.51)$$

$$g = \frac{\partial B_y}{\partial x} = \frac{\partial B_x}{\partial y} = \frac{B_0}{R_0} b_2 . \quad (1.52)$$

In the air space of the quadrupole we have

$$\mathbf{B} = -\nabla\Phi \text{ with } \Phi(x,y) = -g xy . \quad (1.53)$$

The equipotential lines are the hyperbolas $xy = \text{const.}$ The field lines are perpendicular to them.

As shown from the force vectors represented on Fig. 1.39, a single quadrupole will focus the beam in one direction (in this case the direction y) whereas defocussing the beam in the other. At this point we could ask ourselves how an overall focusing in both direction can be achieved. This is performed by creating a so-called FODO lattice, consisting of a focusing (say in the y direction) F quadrupole, a drift space O, a defocussing (in the y direction) D quadrupole and again a space O, which is called a quadrupole doublet (see Exercises).¹⁸

We can calculate the focal length of a quadrupole (see Fig. 1.41). If L denotes the length of the quadrupole, the deflection angle for a particle flying in the beam direction at a distance $y = R$ from the central axis is given by (using Eqs. 1.50 and 1.36 and considering the thin lens approximation):

$$\alpha \simeq \frac{L}{r} = \frac{eB_x}{p}L \simeq \frac{egR}{p}L . \quad (1.54)$$

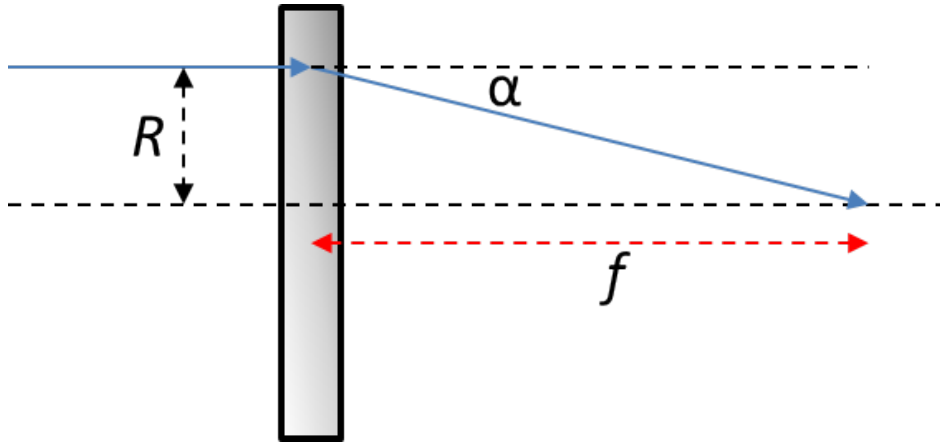


Figure 1.41.: Schematic of the focal length of a focusing quadrupole.

The focal length f is therefore:

$$\alpha \simeq \frac{R}{f} \rightarrow \frac{1}{f} = \frac{eg}{p}L = kL , \quad (1.55)$$

¹⁸Note that the FODO is used as a general name for a focusing lattice and that the magnet arrangement can be more complicated.

where we have defined the quadrupole strength $k = eg/p$ which normalizes the field gradient to the momentum of the particle (in analogy to the bending strength $1/r$ defined in Eq. 1.36). And numerically we have:

$$k [\text{m}^{-2}] = 0.2998 \frac{g [\text{T/m}]}{p [\text{GeV}/c]} . \quad (1.56)$$

1.8.3.3. Separator (Wien filter) and spin rotator As seen above, the momentum selection performed by the first bending magnet does not differentiate between different types of particle having the same momentum. This task is performed downstream by a “separator” or better say a “Wien filter”.

A Wien filter is a device where perpendicular electric and magnetic fields are applied. It can be used as a velocity filter for charged particles.¹⁹ The particles with the right speed will not be affected by the fields (*i.e.* will sense a Lorentz force equal to zero) while other particles will be deflected. It is named after Wilhelm Wien.

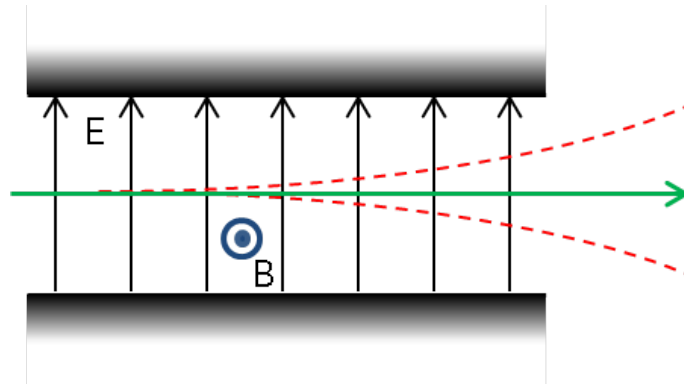


Figure 1.42.: Schematic of a Wien filter. The particles following the green trajectory will have the chosen velocity. The one with a lower (higher) velocity will be deflected on the top (bottom) of the figure.

The total Lorentz force on a particle with charge e is given by:

$$\mathbf{F} = e\mathbf{E} + e\mathbf{v} \times \mathbf{B} \quad (1.57)$$

Here, the vectors \mathbf{v} , \mathbf{E} and \mathbf{B} are orthogonal and therefore the “electrical” part and the “magnetic” part of the Lorentz force are pointing into opposite directions. Therefore the central trajectory will be followed by particles having the velocity

$$v = \frac{E}{B} , \quad (1.58)$$

¹⁹In addition to muon beams, Wien filters can be used for electron microscope or in accelerator mass spectrometry.

meaning that any combination of electric and magnetic fields will allow charged particles with only velocity through.²⁰

Although the trajectory of the muons having the chosen velocity is not altered with the correct ratio between the electrical and magnetic fields, the magnetic field applied will change the orientation of the muon spin compared to the trajectory following Eq. 1.34. For a beam of surface muons, the angle introduced by the Wien filter (used as a separator) is typically of the order of 5-10°. This small spin rotation results in a polarization loss of the order of 1%.

A Wien filter can be used for surface-muon beams (see Section 1.8.3.2) and low-energy-muon beams (see Section 7). However, it cannot be used for high-energy muon beams as a separation between muons and positrons would be ineffective with reasonable fields. For a surface muon beam, the electrodes creating the electrical field have a gap of typically 0.2 m and one applies a voltage difference of about 80 kV.

For some μ SR experiments, it could be very convenient to apply at the sample position a magnetic field perpendicular to the muon spin direction (see Section 3.4.2). For high-energy muon beams, the magnetic field is applied transverse to the muon momentum direction at the sample position. This solution cannot be adopted for the other beams, as the magnetic field would dramatically influence the beam trajectory due to the reduced velocity.²¹ For these beams, the solution is to rotate the muon spin to 90° (or close to this value) with respect to the momentum direction prior to send the muon into the sample. This can be achieved by a Wien filter (used here as a “spin-rotator”) but using much higher magnetic field (and consequently much higher electrical field to select the correct trajectory) resulting to a much higher spin rotation than the one achieved in separator mode.²²

A typical “spin-rotator” (*i.e.* a Wien filter used to rotate the muon-spin) has a length of say about 3 m and can rotate the spin by typically 45 to 65°. For a complete 90° rotation a FODO (quadrupole doublet) is usually introduced in-between two Wien-filters to increase the overall transmission. The typical voltage used for the electrical field are of the order of 500 kV difference and, as the muon beam is in vacuum, requires special technology for the feedthroughs.

²⁰Note that here we stuck with the classical case. In the reality for muons with a high momentum, a static electrical field will also be seen as a magnetic field and corrections to the given formula will be necessary.

²¹Note that even for high-energy muon beams the influence on the muon trajectory of the applied magnetic field at the sample site is not negligible and precise sample and detector position corrections have to be applied. These corrections will depend on the applied value of the magnetic field and on the value of the muon momentum.

²²The use of a spin-rotator is not possible in high-energy beams due to the large velocity of the particles.



Figure 1.43.: *Typical spin rotators installed in the $\pi E3$ beamline of the Paul Scherrer Institute.*

2. Implanting Muons in Matter

2.1. Energy loss of particles in matter

The stopping power of particles in matter occurs by radiative and collision processes with probabilities given by their interaction cross sections. What one observes is a statistical average of the two processes occurring as the particle slows down.

One defines the “Energy Loss” (or stopping power) which is given by

$$-\frac{dE}{d\ell} \quad (2.1)$$

where E is the charged particle kinetic energy. The SI units of stopping power are J/m, but as usual in particle physics the energy is normally given in eV. The higher the stopping power, the shorter the range into the material the particle can penetrate. The negative sign expresses the loss of energy. As the energy loss is proportional to the material density, one often scales it to the density ρ :

$$-\frac{dE}{d\ell} \frac{1}{\rho} = -\frac{dE}{dx} \quad (2.2)$$

with $x = \ell\rho$ (with the units [g/cm²]) and therefore the energy loss is often expressed in eV cm²/g.

After a relatively well-defined distance, called the “range”,¹ the particles will come at rest having lost all their kinetic energy. At the end of the range, the energy loss can no more be considered as continuous and the individual encounters are important. For electrons, this can lead to a significant statistical variation in path length, but for muons or protons (and other heavy particles) with kinetic energies of several MeV or more, one observes path length variations of only a few percent or less, for identical monoenergetic particles. The statistical variation of the path lengths is called the “straggling”.

They are many different types of interactions and the dominating processes will depend on the particle type and on their energy.

Photon: The main energy losses processes are:

¹Note that the range is often given with the units g/cm² which corresponds to the distance range (or mean penetration depth) normalized to the material density i.e. L/ρ .

- The photoelectric effect, which is the emission of electrons resulting from the transfer of energy from the light to an electron. This is a low-energy phenomenon.
- Compton scattering (that is the inelastic scattering of a photon by a charged particle, usually an electron).
- Thomson scattering (which can be seen as the low-energy limit of the Compton scattering) is the elastic scattering of electromagnetic radiation by a free charged particle.
- And finally the pair production which is the creation of an elementary particle and its antiparticle from the neutral photon. This can be seen as a high-energy phenomenon.

Charged particles: The main mechanisms are: Bremsstrahlung, Cherenkov effect radiation, ionization and excitation.

- The Bremsstrahlung is the radiation produced by the deceleration of a charged particle deflected by the field of a target charged particle. The energy loss of a charged particle emitting Bremsstrahlung is proportional to

$$\frac{Z^2 E}{m^2} . \quad (2.3)$$

This proportionality is the reason that light particles such as electrons can intensively emit Bremsstrahlung. On the other hand, muons will generate Bremsstrahlung with a probability more than four orders of magnitude lower. Actually, for all particles other than electrons or positrons, Bremsstrahlung is negligible at energies below 1 TeV (see also Fig 2.4).

- The Cherenkov effect is the radiation emitted when a charged particle travels in a medium faster than the speed of light in that medium (*i.e.* at a speed higher than c/n (where n is the refraction index which has typical values around 1.5 in liquids or solids)). The Cherenkov effect is similar to the ‘supersonic boom’ of a plane flying faster than the speed of sound. The electric field of the ‘slowly’ flying charged particle will polarize the medium by disrupting the local electromagnetic field. After the particle has passed, the medium relaxes to its original unpolarized state. This change of polarization in the medium represents an electromagnetic perturbation that will propagate at the speed of light in the medium. Therefore, far away from the particle’s trajectory, the perturbations will arrive randomly and annihilate each other. On the other hand if the particle travels at a speed faster than the speed of light in the medium, then the small electromagnetic perturbations caused by the polarization and depolarization of the medium propagate less rapidly than the particle and will form together one wavefront. This wave will propagate in a direction given by the speed of the particle and the speed of light in the medium.

The energy loss contributions due to Cherenkov radiation are small (of the order of 1% to the usual energy loss).

- For the muons we are interested for (having a speed of the order of $0.3c$), the main channel of energy loss is the transfer of energy to electrons leading to ionization or excitation of electrons on upper shells.² The number of these collisions is large in dense materials and the cross section of these collisions is large ($\sigma \sim 10 \times 10^{-13} \text{ m}^2$) but of course the energy loss is very small per collision.

If the energy of the particles is large compared with the ionization energies, the energy loss in each ‘collision’ with an electron will be only a small fraction of the particle’s energy. As the number of electrons in matter is so large, we can treat the loss of energy as continuous.

Hadrons: As seen with the collision of the proton with a nucleus which produces pions, here an additional mechanism is inelastic nuclear interactions, which can produce (as seen) pions, kaons, protons, neutrons or fragment of nucleus.

The history of the energy loss calculation is first marked by the works of Bohr in 1913 and 1915 [22, 23]. In 1930, the quantum mechanical version (first non-relativistic, then relativistic) was proposed by Bethe [24]. The Bethe’s formulation is based using quantum mechanical perturbation theory.

2.1.1. Energy loss by ionization: classical approach

We first derive the classical formula for the interaction particle/electron. This represents the Bohr formulation of the interaction.

²Note that in general, the elastic collisions between muons and nucleus can be safely neglected as (in the classical limit) the maximum energy transfer in an elastic collision is given by:

$$\begin{aligned}\Delta E_{\text{max}} &= \frac{1}{2}mv^2 \left(\frac{4mM}{(m+M)^2} \right) \\ &= \frac{2Mv^2}{1 + 2\frac{M}{m} + \frac{M^2}{m^2}}\end{aligned}\tag{2.4}$$

and therefore negligible for $M \gg m$.

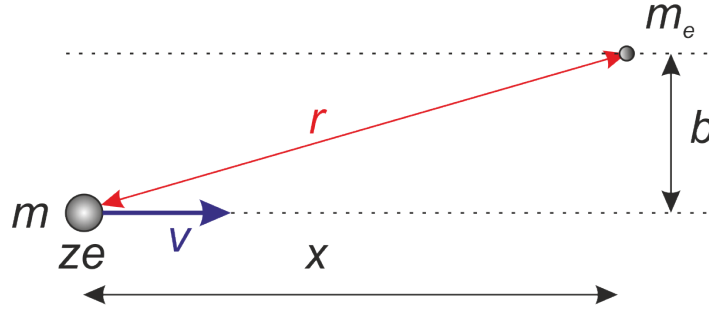


Figure 2.1.: Model for calculating the energy lost by a charged particle in a collision with an electron. The parameter b is called the impact parameter.

The momentum transferred to the electron (supposed at rest prior the interaction) is equal to

$$\Delta p = \int_{-\infty}^{\infty} F_{\text{Coul}} dt . \quad (2.5)$$

For the Coulomb force, we only have to consider the transversal component, as the contribution from the longitudinal part will cancel out.

$$F_{\text{Coul}}^{\perp} = F_{\text{Coul}} \frac{b}{r} = F_{\text{Coul}} \frac{b}{\sqrt{b^2 + x^2}} = \frac{kze^2}{b^2 + x^2} \frac{b}{\sqrt{b^2 + x^2}} \quad (2.6)$$

where k is the Coulomb constant (value dependent on the units chosen) and ze is the charge of the flying particle. Therefore

$$\Delta p = \int_{-\infty}^{\infty} \frac{kze^2}{b^2 + x^2} \frac{b}{\sqrt{b^2 + x^2}} \frac{dx}{v} , \quad (2.7)$$

where v is the velocity and we get

$$\Delta p = \frac{2kze^2}{vb} , \quad (2.8)$$

and therefore the energy transfer in one encounter is

$$\Delta E(b) = \frac{\Delta p^2}{2m_e} = \frac{2k^2 z^2 e^4}{m_e v^2 b^2} . \quad (2.9)$$

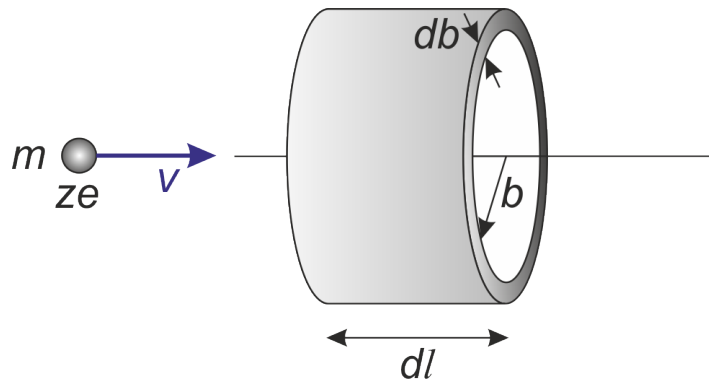


Figure 2.2.: In path length dl , the charged particle collides with the electrons with impact parameters in db .

To find how many encounters occur, we consider a cylindrical volume of thickness db and length $d\ell$ (see Fig. 2.2). There are

$$\frac{ZN_A}{A} \rho \, 2\pi \, db \, d\ell \quad (2.10)$$

electrons in this volume, where Z is the atomic number, A the atomic weight, N_A the Avogadro's number, and ρ the mass density. The total energy lost to these electrons is then

$$\Delta E = \frac{2k^2 z^2 e^4 Z N_A}{m_e v^2 A b^2} \rho \, 2\pi b \, db \, d\ell \quad (2.11)$$

We have to remember that Eq. 2.11 is for the volume dV of thickness db and therefore we have to integrate from a minimum to a maximum value of b . Hence, we have now to identify the maximum and minimum value of the impact parameter b .

For one encounter, the maximum energy transfer is $\Delta E_{\max} = 2m_e v^2$ (consider Eq. 2.4 with $M = m_e \ll m$). These collisions are usually called “hard” collisions. In some of the hard collisions the atomic electron acquires such a large energy that it causes secondary ionisation. We have

$$\Delta E_{\max} = 2m_e v^2 = \Delta E(b_{\min}) = \frac{2k^2 z^2 e^4}{m_e v^2 b_{\min}^2} \quad \text{and so} \quad (2.12)$$

$$b_{\min} = \frac{kze^2}{m_e v^2} \quad (2.13)$$

The minimum value of the energy transfer correspond to the so-called “mean excitation energy”, *i.e.* $\Delta E_{\min} = I$. These collisions are usually called “soft” collisions. The value of I is not something that can be easily calculated and usually it has to be determined experimentally. It can be approximate (for $Z > 1$) by

$$I = 16 \text{ eV} \times Z^{0.9} \quad (2.14)$$

and for $Z > 20$ by

$$I = 10 \text{ eV} \times Z \quad (2.15)$$

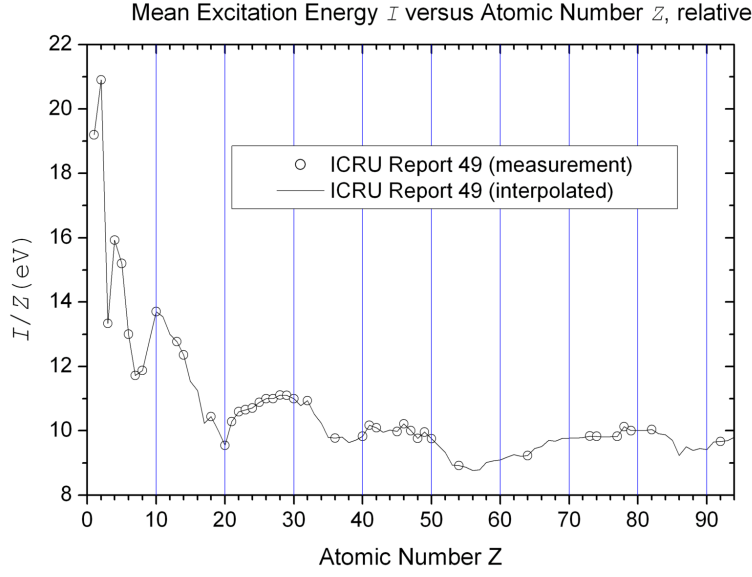


Figure 2.3.: Mean potential energy determined experimentally. (Taken from <https://de.wikipedia.org/wiki/Bethe-Formel>.)

We can write therefore

$$\Delta E_{\min} = I = \Delta E(b_{\max}) = \frac{2k^2 z^2 e^4}{m_e v^2 b_{\max}^2} \quad \text{and so} \quad (2.16)$$

$$b_{\max} = \frac{kze^2}{v} \sqrt{\frac{2}{m_e I}}. \quad (2.17)$$

We recall that $dx = \rho d\ell$ and we have (introducing a negative sign to take into account the loss of energy for the incoming particle)

$$-\frac{dE}{dx} = \int_{b_{\min}}^{b_{\max}} \frac{2k^2 z^2 e^4 Z N_A}{m_e v^2 A b} 2\pi db = \frac{4\pi k^2 z^2 e^4 Z N_A}{m_e v^2 A} \frac{1}{2} \ln\left(\frac{2m_e v^2}{I}\right) \quad (2.18)$$

$$= \frac{4\pi k^2 z^2 e^4 Z N_A}{m_e \beta^2 c^2 A} \frac{1}{2} \ln\left(\frac{2m_e \beta^2 c^2}{I}\right), \quad (2.19)$$

(where we have introduced $\beta = v/c$) which represents the Bohr classical derivation of the Bethe formula.

In cgs units we have $k = 1$ and the energy loss is as said expressed in eV cm²/g.

2.1.2. Energy loss: Bethe formula

As said, Bethe performed the full quantum mechanical derivation, and obtained:

$$-\frac{dE}{dx} = \frac{4\pi k^2 z^2 e^4 Z N_A}{m_e \beta^2 c^2 A} \left(\frac{1}{2} \ln \frac{2m_e \beta^2 c^2 \gamma^2 T_{\max}}{I^2} - \beta^2 - \frac{\delta(\beta\gamma)}{2} \right). \quad (2.20)$$

The term T_{\max} represents the maximum kinetic energy transfer onto one electron calculated relativistically and is given by:

$$T_{\max} = \frac{2m_e c^2 \beta^2 \gamma^2}{1 + 2\gamma \frac{m_e}{m} + \frac{m_e^2}{m^2}}, \quad (2.21)$$

where $\gamma = (1 - \beta^2)^{-1/2}$ is the Lorentz factor.

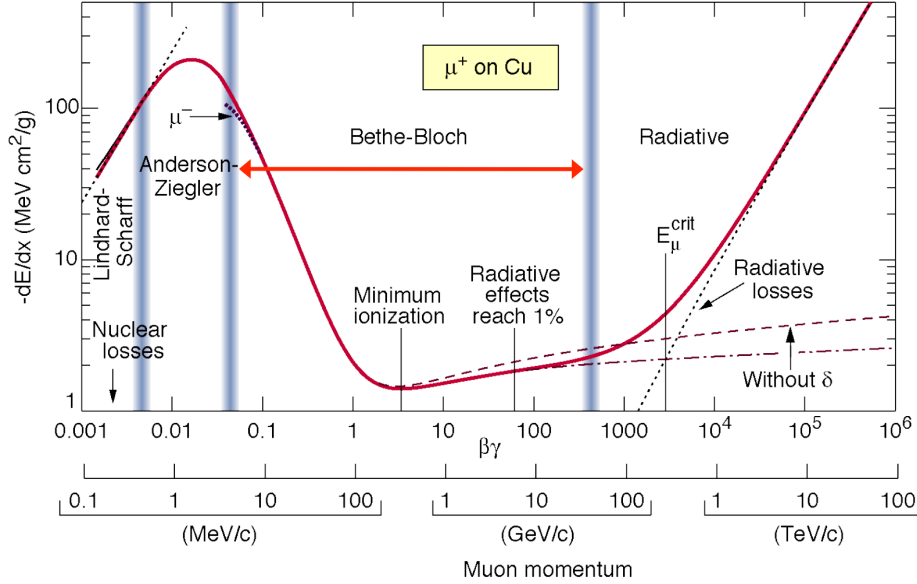


Figure 2.4.: Stopping power $-dE/dx$ for positive muons in copper as a function of $\beta\gamma = p/(mc)$ over nine orders of magnitude. The validity range of the Bethe formula is indicated [25]. There are two regions where the Bethe formula is no more valid. First at high velocity, the radiation effects are the result of Bremsstrahlung which becomes important here in reason of the kinetic energy (see Eq. 2.3). On the other side at low velocity, one observes a linear increase of the stopping power. For these low energies, a positively charged particle can pick-up an electron and therefore its effective charge, and therefore the stopping power, will be reduced. By increasing the velocity, this effect will decrease as the probability to pick-up an electron will decrease. Alternatively, if the flying particle is an ion with electrons, these will be stripped with a probability which grows with velocity [26].

They are few important points concerning this formula:

- In the range where the Bethe formula is valid, we have three different regions :
 1. At low energies a $(1/\beta)^2$ (kinematic factor) drop to a minimum at about $\beta \sim 3 - 4$.
Particles at this point are called minimum ionising particles (“MIP”).
For low energies and when the mass of the incoming particle is bigger than the electron one, we have $\gamma m_e \ll m$ and therefore

$$T_{\max} \simeq 2m_e c^2 \beta^2 \gamma^2. \quad (2.22)$$

Introducing that in the Bethe formula we see that (assuming $\gamma \simeq 1$) the Bethe result corresponds to the classical result except a factor of 2.³

By looking at the Fig 2.4, we see that a muon at the MIP point loses about 13 MeV/cm in copper (density 8.94 g/cm³).

2. At higher energies a logarithmic rise follows, which is due to relativistic effects. It reflects the relativistic increase of the transversal component of the electrical field (Lorentz transformation of the field). This leads to larger collision distances and therefore to more collisions.
 3. At very high energies a plateau is reached. This is due to the density effect. In high density material, the electric field will be partially shielded due to the polarization. Therefore, we have effectively some cuts of the long range contributions. These are of course more relevant at high γ (see the previous point).
- An important point is that the stopping power dE/dx is marginally dependent of the target material (actually only the factor Z/A depends on the material, which is constant over a large range of materials).

³This factor arises from the fact that the classical limit does not describe correctly the very far collisions and that the binding of the electrons cannot be neglected.

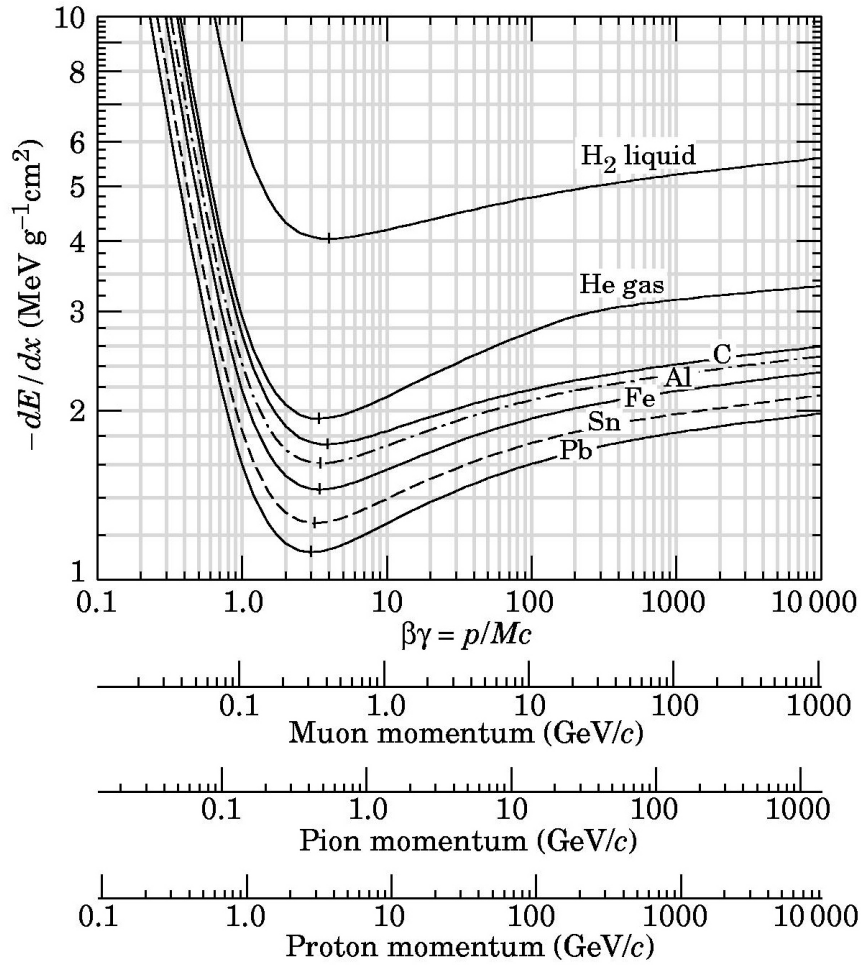


Figure 2.5.: Stopping power $-dE/dx$ in liquid hydrogen, helium gas, carbon, aluminum, iron, tin and lead. Except in hydrogen, particles of the same velocity have similar energy loss in different materials [25].

- The Bethe equation does *not* depend on the mass of the incoming particle. This means that it is an universal curve as a function of $\beta\gamma$ for particles with the same charge. However the stopping power “split up” for different particle masses if taken (or measured) as a function of the incoming momentum or energy.

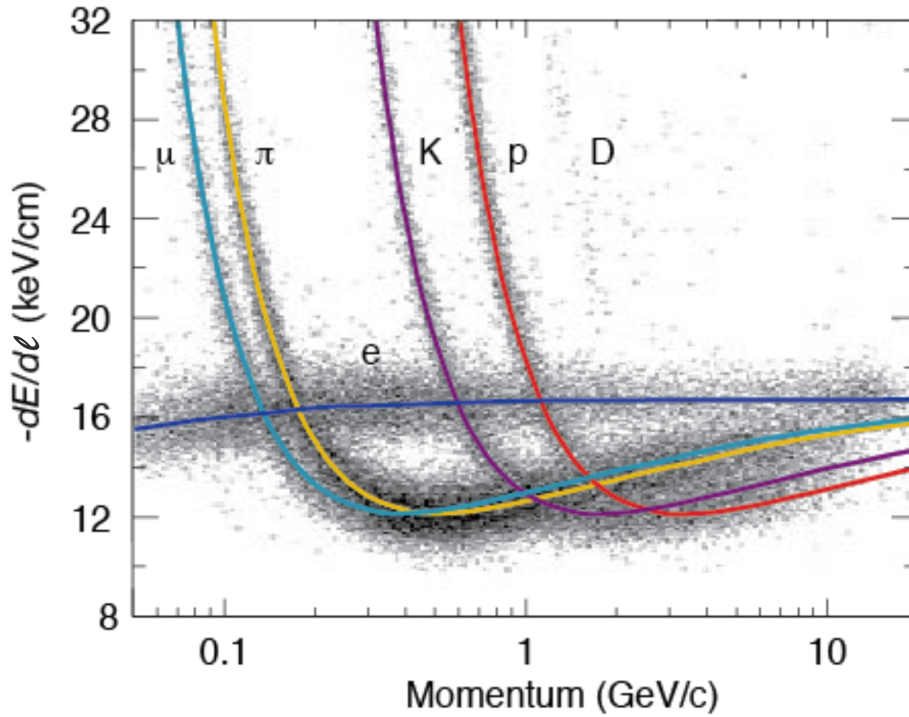


Figure 2.6.: Stopping power $-dE/d\ell$ in a mixture of argon (80%) at 8.5 bar reported as a function of the particle impulse. The electron stopping power does not follow the Bethe formula (Bremsstrahlung dominant). Adapted from Manfred Krammer [27].

- The energy loss is a statistical process. Hence the number of collisions and energy loss varies from particle to particle. Also the distribution of stopping depth is usually asymmetric. This reflects the fact that collisions with a small energy transfer are more probable than those with a large energy transfer. A result of the asymmetric distribution is that the mean energy loss is larger than the most probable energy loss. The energy loss as function of the penetration depth is called the “Bragg Curve” (or Bragg peak). The fact that the energy loss is maximum just before the particle comes to a complete stop is used in particle therapy of cancer, to concentrate the effect of ion beams on the tumor while minimizing the effect on the surrounding healthy tissue.

This property is used for so-called proton therapy, for example at the Paul Scherrer Institute.

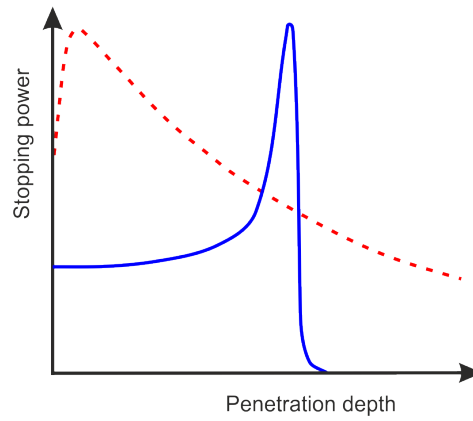


Figure 2.7.: Schematic of the stopping power for photons (red) and protons (blue) as a function of the penetration depth.



Figure 2.8.: Proton therapy treatments at PSI use an in-house built superconductor accelerator, a compact cyclotron, called COMET. It was especially developed for medical applications by the company ACCEL (now part of Varian Medical Systems) and brought into service in 2007. It delivers a beam energy of 250 MeV, which can be reduced when needed for patient treatments (see <https://www.psi.ch/protontherapy/center-for-proton-therapy-cpt>).

2.2. Range and thermalization time

2.2.1. Range of muons

The range R (in g/cm^2) is given by the integration

$$\begin{aligned} R &= \int_{E_{\text{kin}}}^0 \frac{1}{dE/dx} dE \\ &= \int_{E_{\text{tot}}}^{mc^2} \frac{1}{dE/dx} dE . \end{aligned} \quad (2.23)$$

We can also define the range in length units (say cm) for a given material as

$$\begin{aligned} R_\ell &= \frac{R}{\rho} \\ &= \frac{1}{\rho} \int_{E_{\text{tot}}}^{mc^2} \frac{1}{dE/dx} dE . \end{aligned} \quad (2.24)$$

Within its validity range, the integration should be performed with the Bethe-Bloch formula, which is a hard task due to the logarithmic term. Often one considers some approximations for the different ranges. For example for a muon having an initial impulse $p = \gamma mv = \beta \gamma mc$, one often uses:

$$-\frac{dE}{dx} = \begin{cases} a \frac{\ln(\beta)}{\beta^2}, & \text{for } \beta\gamma = \frac{p}{mc} \ll 1 \\ b \frac{1}{\beta^2}, & \text{for } \beta\gamma = \frac{p}{mc} \lesssim 1 \\ c, & \text{for } \beta\gamma = \frac{p}{mc} \simeq 3 - 4 \\ c + d \ln(\beta), & \text{for } \beta\gamma = \frac{p}{mc} \gg 1 \end{cases} \quad (2.25)$$

We have seen that for high energy beamlines we use backward muons with high impulse (see Fig. 1.32). For these impulses we can use the second condition and therefore:

$$-\frac{dE}{dx} = b \frac{1}{\beta^2} , \quad (2.26)$$

with $b \simeq 1.5 \text{ MeV}/(\text{g}/\text{cm}^2)$. We therefore have (see Exercises for details)

$$\begin{aligned}
 R &= \int_{E_{\text{tot}}}^{mc^2} \frac{1}{dE/dx} dE \\
 &= \int_{E_{\text{tot}}}^{mc^2} -\frac{\beta^2}{b} dE \\
 &= \dots \\
 &= \frac{1}{b} \frac{(\gamma - 1)^2}{\gamma} mc^2 .
 \end{aligned} \tag{2.27}$$

For a muon with an impulse $p = 110 \text{ MeV}/c$ (that is a total energy of about 152.5 MeV and $\gamma \simeq 1.444$) one gets a range of $R \simeq 9.5 \text{ g}/\text{cm}^2$. For copper ($\rho_{\text{Cu}} = 8.96 \text{ g}/\text{cm}^3$) this represent a penetration of the muon to $R_\ell = \frac{R}{\rho_{\text{Cu}}} \simeq 1.1 \text{ cm}$.

For the lower impulse (as the one present in surface muon beams), the above formula underestimates the true range by a fair amount. This is the consequence of having neglected the logarithmic term in the stopping power.

For surface muon beams with a momentum of the order of $p \simeq 30 \text{ MeV}/c$ and a typical momentum bite of $\Delta p/p \simeq 0.03$, the range R is of the order of $130 \text{ mg}/\text{cm}^2$ and the straggling ΔR is about 13% of R .

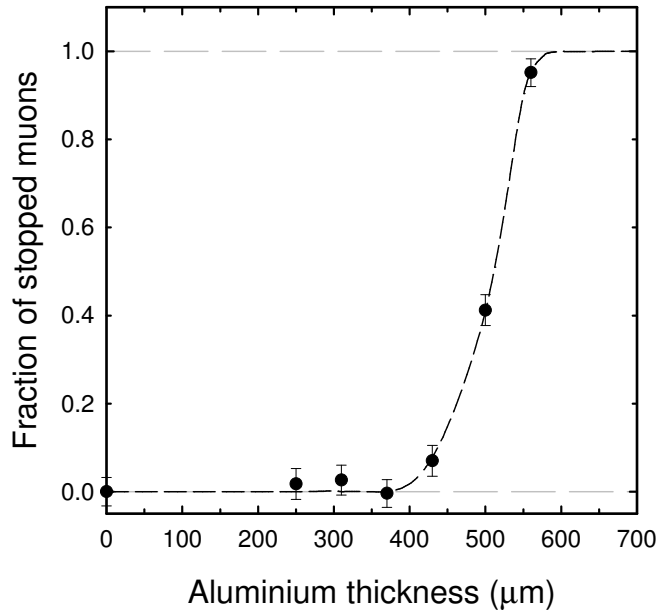


Figure 2.9.: Fraction of the muon beam stopped as a function of the aluminium sample thickness. The measurements were performed at the GPS instrument at PSI using surface muons. For thin samples, the muons are flying through the sample. The full beam is typically stopped by an aluminum sample with a thickness of about $L = 0.50 \pm 0.05 \text{ mm}$, which corresponds to a range of $R = L\rho \simeq 135 \text{ mg}/\text{cm}^2$.

Analog to what we saw for the proton therapy, the muons will present a Bragg peak (see Fig. 2.7). We can roughly determine the shape of the Bragg curve, by starting from Eq. 2.26. The loss of kinetic energy will be

$$-\frac{dE}{dx} \simeq \frac{d}{dx} \left(\frac{1}{2} m \beta^2(x) c^2 \right) , \quad (2.28)$$

neglecting the relativistic character. Therefore

$$\begin{aligned} -\frac{d}{dx} \left(\frac{1}{2} m \beta^2(x) c^2 \right) &= \frac{b}{\beta^2(x)} \\ -mc^2 \beta(x) \frac{d\beta}{dx} &= \frac{b}{\beta^2(x)} \\ -\beta^3(x) d\beta &= \frac{b}{mc^2} dx \\ \beta^4(x) - \beta_0^4 &= -\frac{4b}{mc^2} x \\ \beta^2(x) &= \beta_0^2 \sqrt{1 - \frac{4b}{mc^2 \beta_0^4} x} \\ \beta^2(x) &= \beta_0^2 \sqrt{1 - \frac{x}{R}} . \end{aligned} \quad (2.29)$$

Using now this dependence of $\beta(x)$, we can rewrite Eq. 2.26 as

$$-\frac{dE}{dx}(x) = \frac{b}{\beta_0^2 \sqrt{1 - \frac{x}{R}}} . \quad (2.30)$$

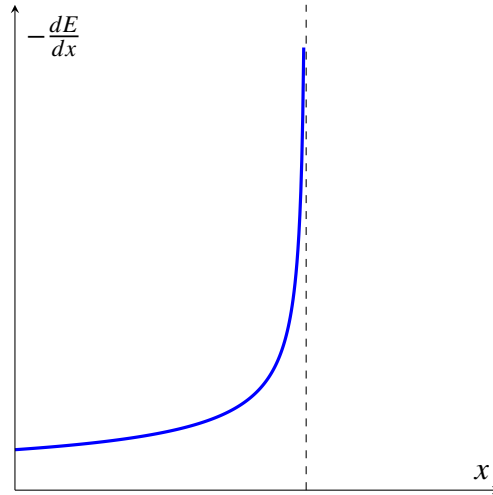


Figure 2.10.: Rough estimate of the Bragg curve obtained with Eq. 2.30. The real maximum occurs before the full range is reached (see text and Fig. 2.7).

This is of course a rough estimation as the stopping power will not follow Eq. 2.26 for all the velocities. Overall, the Bragg curve is much less peaked than predicted by Eq. 2.30 and its maximum occurs before the full range is reached.

2.2.2. Thermalization time

The thermalization time is given by:

$$\begin{aligned} t_{\text{th}} &= \int_{E_{\text{in}}}^0 dt = \int_{E_{\text{in}}}^0 \frac{d\ell}{v} = \int_{E_{\text{in}}}^0 \frac{1}{v \frac{dE}{d\ell}} dE \\ &= \int_{E_{\text{in}}}^0 \frac{1}{v\rho \frac{dE}{dx}} dE . \end{aligned} \quad (2.31)$$

We see that this time is proportional to the inverse of the density and is of the order of ~ 10 ps for usual solids.

2.3. “Free” muon vs muonium

After its deceleration, the positive muon actually represent a charged impurity which will be generally located at an interstitial position in the crystal lattice. In a metal, its charge will change the local charge density of the conduction electrons.

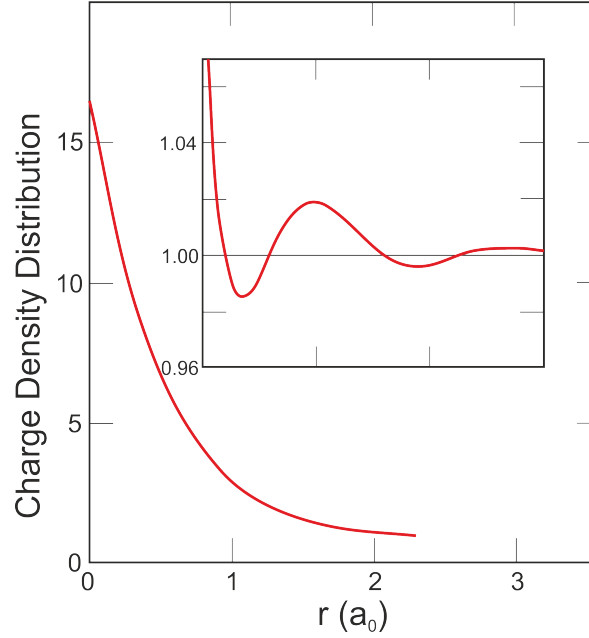


Figure 2.11.: Typical normalized electron charge-density distribution around the positive muon (adapted from [28]). The solid curve corresponds to the normalized charge density $n(r)/n_0$ (see text). The exact form will depend on the density of the conduction electrons with obviously $n(r=0)/n_0$ increasing strongly for large values of r_s .

One can define the unperturbed electron density as n_0 writing

$$n_0 = \frac{1}{\frac{4}{3}\pi(r_s a_0)^3} , \quad (2.32)$$

where a_0 is the Bohr radius and r_s is conventionally being referred to as the electron density parameter. So $r_s a_0$ represents the radius of a sphere containing one electron.

The unperturbed electron density is obtained by taking typically $r_s = 2$ giving

$$n_0(r_s) = \frac{1}{\frac{4}{3}\pi(2a_0)^3} . \quad (2.33)$$

The Fig. 2.11 shows us that in the presence of the muon we have quite an increase at the muon site ($r = 0$) with

$$n(r=0) \simeq 16 \times n_0 = \frac{16}{\frac{4}{3}\pi(2a_0)^3} . \quad (2.34)$$

We note that the electron density for muonium corresponds to the situation with $r_s = 1$ (the Bohr radius for the muonium is almost identical to the one for hydrogen; see Section ??) and therefore the electron density at the muon site in a metal is only twice the one in muonium as

$$n_{e,\text{Mu}} = \frac{1}{\frac{4}{3}\pi a_0^3} \simeq \frac{1}{2} n(r=0) . \quad (2.35)$$

In spite of this, muonium is not observed in metal. The collective screening of the muon Coulomb potential will impede the formation of a bound state muon-electron. Even if the state is shortly formed, it will be extremely short lived and will be destroyed by the scattering of the bound electron with the conduction electrons.

Therefore the positive muon implanted into a metal will behave as a “free” muon (so-called diamagnetic state).

A very important point is that the involved slowing-down processes are only electrostatic, and therefore, the muon polarization will not be affected.

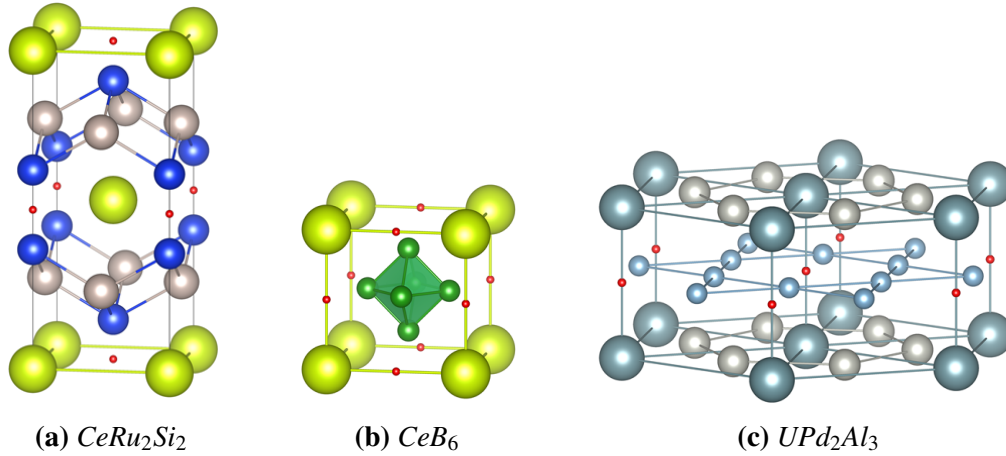


Figure 2.12.: Examples of muon stopping sites (red spheres) determined experimentally for different systems. For each system, the sites are crystallographically equivalent.

The story is different in materials where the free-electron density is low as insulators, semi-conductors, molecular systems, liquids or gases. In these system the muon can pick-up an electron and form muonium (see Section 8). Actually a limit on the electron density to observe muonium in a material was given by Estreicher and Meier [29] with $n \sim 3 \times 10^{22} \text{ cm}^{-3}$. In these materials, when the kinetic energy of the implanted muons has dropped to several tens of keV, *i.e.* when the muon velocity becomes comparable to the orbital velocity of electrons of the medium, then the positive muon can pick-up an electron to form a muonium. Generally, the muon will be stripped of this electron but can bind again with another one. The muon undergoes a rapid series of several hundred electron pickup and stripping cycles, loosing energy at each cycle. If the last step before a complete thermalization leaves intact the muonium, then one speaks of “prompt” formation. On the other side if the muon thermalizes as a bare particle and subsequently pick-up an electron, the formation is called “delayed”.

